Published in final edited form as:
Sci Signal. ; 11(526): . doi:10.1126/scisignal.aap8112.

Interleukin-2 shapes the cytotoxic T cell proteome and immune environment-sensing programs

Christina M. Rollings[1], **Linda V. Sinclair**[1], **Hugh J. M. Brady**[2], **Doreen A. Cantrell**[1,*], and **Sarah H. Ross**[1,*]

[1]Division of Cell Signalling and Immunology, School of Life Sciences, University of Dundee, DD1 5EH, United Kingdom

[2]Department of Life Sciences, Imperial College London, London, SW7 2AZ, UK

Abstract

Interleukin-2 (IL-2) and Janus kinases (JAKs) regulate transcriptional programs and protein synthesis to promote the differentiation of effector $CD8^+$ cytotoxic T cells (CTLs). Using high-resolution mass spectrometry, we generated an in-depth characterization of how IL-2 and JAKs configure the CTL proteome to control CTL function. We found that IL-2 signaling through JAK1 and JAK3 (JAK1/3) increased the abundance of a key subset of proteins to induce the accumulation of critical cytokines and effector molecules in T cells. Moreover, IL-2 maintained the concentration of proteins that support core metabolic processes essential for cellular fitness. One fundamental insight was the dominant role for IL-2 in stimulating effector T cells to detect microenvironmental cues. IL-2-JAK1/3 signaling pathways thus increased the abundance of nutrient transporters, nutrient sensors, and critical oxygen-sensing molecules. These data provide key insights into how IL-2 promotes T cell function and highlight signaling mechanisms and transcription factors that integrate oxygen sensing to transcriptional control of $CD8^+$ T cell differentiation.

Introduction

Interleukin-2 (IL-2) is a member of the γ_c cytokine family, which activate receptors containing the common γ_c subunit. IL-2 has numerous roles in orchestrating immune responses, including stimulating the proliferation and differentiation of CD4+ and $CD8^+$ effector T cells (1–5). This vital role in controlling T cell fate has made manipulation of IL-2 signaling an attractive aim for immunotherapies. Hence, IL-2 was one of the first cytokines used in immunotherapy to increase T cell responses. IL-2 is also used to expand tumor-specific T cells and chimeric antigen receptor-redirected T cells (CAR-T cells) ex vivo before adoptive transfer into patients (6, 7). IL-2 signals through the tyrosine kinases JAK1

*Correspondence should be addressed to D. A. Cantrell (d.a.cantrell@dundee.ac.uk) or S.H. Ross (s.t.ross@dundee.ac.uk).

Author contributions: C.M.R. and S.H.R. designed, performed, and analyzed experiments; L.V.S and S.H.R provided training; H.J.M.B supplied mice. D.A.C. and S.H.R. designed the project and wrote the manuscript with intellectual input from C.M.R.

Competing interests: The authors declare that they have no competing interests.

Data and materials availability: The proteomics data are available via the ProteomeXchange Consortium (http://proteomecentral.proteomexchange.org) via the PRIDE repository with the dataset identifier PXD008112.

Europe PMC Funders Author Manuscripts

and JAK3; hence, inhibitors of both JAK1 and 3 (JAK1/3), such as Tofacitinib, have been developed to modulate IL-2 immunoregulatory pathways to treat autoimmune and inflammatory conditions. Moreover, the pleiotropic role of IL-2 in promoting both proinflammatory effector T cell responses and the anti-inflammatory homeostasis of regulatory T cells has stimulated the development of strategies using modified IL-2 proteins with altered receptor binding (8) and antibodies that target this cytokine (4, 9) to direct IL-2 activity towards specific T cell subsets in order to manipulate IL-2 signaling responses for therapies.

In terms of $CD8^+$ cytotoxic T lymphocytes (CTLs), IL-2 stimulates T cell growth and T cell clonal expansion (6, 10, 11). Thus, IL-2 stimulates transcriptional programs that are required for cell cycle progression and proliferation. IL-2 also stimulates the production of interferon gamma (IFN-γ) and the effector molecules perforin and granzyme and directs the repertoire of adhesion molecules and chemokine receptors present on the plasma membrane of the CTL to promote trafficking to peripheral tissues. The outcome of these regulatory events is that IL-2 directs the differentiation of effector CTLs at the expense of the development of memory $CD8^+$ T cells (12–15).

In order to induce this differentiation, IL-2 activates signal transducer and activator of transcription 5 (STAT5) (3, 16–18) and MYC (19) transcriptional programs. In addition, IL-2-stimulated JAK1/3 activates serine and threonine kinase signaling networks. For example, IL-2 activates mammalian target of rapamycin complex 1 (mTORC1)-mediated signaling pathways, which promote the production of inflammatory cytokines, cytolytic effector molecules, and glucose transporters, and enhance glucose and fatty acid metabolism in CTLs (20–23). Moreover, the IL-2-JAK-regulated phosphoproteome of CTLs is dominated by proteins that control mRNA stability and components of the protein translational machinery (24). Hence, a key role for IL-2 is to sustain protein synthesis in CTLs. Consequently, IL-2 is a “growth factor” for antigen-activated T cells (12, 24, 25). By controlling protein synthesis (24, 25), IL-2 can modify the proteome of CTLs independently from its regulation of gene transcription. One example of this is the ability of IL-2 to stimulate the accumulation of the transcription factor MYC: IL-2 promotes the synthesis of MYC protein without inducing the abundance of *Myc* mRNA (19). Furthermore, IL-2-mediated regulation of mTORC1, which can promote both mRNA translation and cellular protein degradation pathways (23), is another means by which IL-2 can alter the cellular proteome independently from changes in the cell’s transcriptional programs.

Although IL-2 activates JAKs to control T cell transcriptional programs, differences in the rates of protein production - translation and synthesis - and protein degradation - controlled by protein stability and rates of protein degradation - create discordances between the cellular transcriptome and proteome. Hence, determining which proteins are sustained in CTL to control T cell function requires mapping of IL-2-regulated proteomes. Here, we used high-resolution quantitative mass spectrometry to analyze how IL-2 maintains the proteome of differentiated CTLs to generate global and in-depth insights into how this key cytokine controls $CD8^+$ T cell identity and controls cell cycle progression, metabolism, and the abundance of effector molecules.

Results

IL-2 regulation of the CTL proteome

To explore the role of IL-2 on effector $CD8^+$ cytotoxic T lymphocyte (CTL) function, we differentiated lymphocytes from transgenic mice that express a knock-in T cell receptor specific for the gp-33 peptide from lymphocytic choriomeningitis virus (LCMV; P14 mice) (26) into effector $CD8^+$ CTLs by culturing the cells in IL-2. IL-2-maintained CTLs are large granular cells (Fig. 1A) that depend on IL-2 for sustained proliferation and viability. After 24 hours of IL-2 deprivation, CTLs had similar viability to the IL-2-maintained cultures (Fig. 1A) but were decreased in size, as judged by flow cytometry analysis of forward scatter (Fig. 1A). After 48 hours of IL-2 deprivation, cell viability substantially decreased. The decrease in the size of IL-2-deprived CTLs observed by flow cytometry at the 24 hour time point (Fig. 1A) correlated with a reduction in CTL mass (Fig. 1B).

To understand how IL-2 shapes the CTL phenotype, we used quantitative label-free high-resolution mass spectrometry to compare the proteome of CTLs maintained in IL-2 and CTLs deprived of IL-2 for 24 hours (fig. S1A). Identified peptides were matched to a single protein or multiple proteins, termed protein groups, using MaxQuant software (27). We identified more than 6200 protein groups per biological replicate (fig. S1, B and C, table S1), and there was >90% overlap in the proteins identified among the 3 biological replicates (fig. S1, B and C). We converted our label-free data into protein copy numbers per cell using “histone-ruler” methodology (28). The correlation between estimated copy numbers of proteins in different biological replicates of each condition was good; the lowest r2-value was 0.89 (fig. S1, D and E).

Because IL-2-deprived CTLs decreased in both size and mass (Fig. 1A, B) compared to IL-2-maintained CTLs, a key question was whether IL-2 removal resulted in an equal and uniform reduction in all proteins in CTLs. In total, ~6500 proteins were identified in both IL-2-maintained CTLs and IL-2-deprived CTLs (Fig. 1C) with protein abundance spanning several orders of magnitude. Approximately ~3000 proteins were not substantially affected by IL-2 deprivation. The unaffected proteome included cytoskeletal and structural proteins - beta-actin (ACTB), one of the most highly abundant proteins in CTLs, vimentin, and laminin-b - and signaling molecules - the phosphotyrosine phosphatases PTPN6 (SHP-1) and PTPN22 and the guanosine triphosphatase (GTPase) RAP1B (table S1). Futhermore, the abundances of a few proteins were statistically significantly increased in response to IL-2 deprivation (Fig. 1C). Thus, the loss of IL-2 signals did not result in a universal and uniform loss in protein.

Approximately 100 proteins, including histones, cytoskeletal proteins, ribosomal proteins, glycolytic enzymes, and the cytolytic effector molecules granzyme A and granzyme B contributed to ~50% of the mass of IL-2-maintained CTLs (Fig. 1D). IL-2 could control CTL biomass by regulating only the amount of these abundant proteins. However, the overall reduction in the mass of CTLs deprived of IL-2 was between 1.5- and 2-fold (Fig. 1B). Although this decrease included a reduction in some of the abundant proteins, the effect of IL-2 deprivation on the CTL proteome was more complex. We found ~900 proteins that decreased proportionally to the overall loss in mass, indicative of some general cell scaling

down of protein content. However, most IL-2-regulated proteins were changed in abundance by more than 2-fold (Fig. 1C and table S2). A subset of CTL proteins was also highly sensitive to IL-2 deprivation: ~140 proteins became undetectable (table S2), and other proteins changed >20-fold in abundance. These results indicate that the effect of IL-2 on CTL cell mass is not just a simple reduction and scaling down in overall cellular protein content, but a complex reshaping of the proteome.

Dominant effects of IL-2 on the CTL proteome

To understand the dominant consequences of IL-2 deprivation on the CTL proteome, we focused on the proteins that were most decreased in abundance by IL-2 deprivation. Approximately 140 proteins were only reproducibly identified in IL-2-maintained CTLs: These proteins included the effector cytokines lymphotoxin α (LT-α), and IFN-γ (table S2). The cytokine receptor protein TNFRSF9 (also known as CD137 or 4-1BB) was one of the proteins that decreased the most in abundance in CTLs deprived of IL-2. We detected ~300,000 molecules per cell in IL-2-maintained CTLs and ~2000 molecules per cell in IL-2-deprived CTLs (table S2). Other examples of cell surface receptors markedly decreased in abundance by the lack of IL-2 include the IL-4R, IL-12β1, and the inhibitory receptor Tim-3 (also known as HAVCR2) (Fig. 1E). The abundance of IL-2Rα (also known as CD25) subunit is controlled by IL-2 (29), and we identified a 2- to 5-fold reduction in the amount of IL-2Rα after IL-2 deprivation of CTLs (Fig. 1F). This decrease was consistent with the observed changes to IL-2Rα as determined by flow cytometry analysis of the CTLs prior to proteomic analysis (Fig. 1G). We also noted that IL-2Rβ and IL-2Rγ, the other components of the IL-2R, were decreased in IL-2-deprived CTLs (Fig. 1E). Together, the proteomic data highlight the key role for IL-2 in sustaining the abundance of proteins that enable CTLs to respond to external stimuli, including cytokines and inhibitory proteins.

IL-2 regulation of the cell cycle machinery

A quintessential biological function of IL-2 is to control the clonal expansion of antigen receptor-activated T cells. The commitment of T cells to DNA synthesis depends on the activity of cyclin D-cyclin-dependent kinase 2 (CDK2) complexes or cyclin D-CDK4 complexes. We quantified the effect of IL-2 deprivation on the numbers and stoichiometry of the key cell cycle regulators to understand how IL-2 regulates T cell proliferation. We found that IL-2 increased the abundance of cyclin D2 (Fig. 1H) and cyclin D3 (Fig. 1I). Conversely, IL-2 reduced the abundance of the CDK inhibitor CDKN1B (also known as p27 or p27kip) (Fig. 1J). IL-2-deprived CTLs showed increased abundance of CDKN1B molecules relative to the numbers of cyclins D2 and D3 molecules (Fig. 1K). This would result in decreased abundance of active cyclin D-CDK complexes and would be consistent with inhibition of progression through the G1 to S phase of the cell cycle. We also found that IL-2 deprivation caused a decrease in the abundance of essential components of the DNA replication machinery (Fig. 1L), which would limit the ability of CTLs to perform DNA synthesis. IL-2 also sustained the abundance of DNA damage repair proteins (Fig. 1L). Because cyclin D-CDK4 and cyclin D-CDK6 complexes stimulate the activity of the transcription factor E2F, which then stimulates the expression of genes encoding DNA replication proteins (30), the reduction in core DNA synthesis machinery may result from loss of cyclin D-CDK4/6 activity. Thus, our proteomic data indicate that there are multiple

mechanisms by which loss of IL-2 signals limits DNA synthesis and repair in effector T cells, enabling IL-2 to control cell cycle progression and the proliferation of CTLs.

IL-2 regulation of the CTL cytolytic machinery

The key cytolytic effector molecules of CTLs are perforin, granzymes, and FAS ligand, all of which are stored in granules. Granules are specialized secretory lysosomes, which, like other lysosomes, are positive for the lysosomal proteins LAMP-1 (also known as CD107a) and LAMP-2 (31). IL-2 did not substantially affect LAMP-1 and LAMP-2 abundance in CTLs (Fig. 2, A and B). However, cells deprived of IL-2 exhibited a reduction in the abundance of the cytolytic granule cargo molecules perforin, granzyme A, and granzyme B (Fig. 2, C to E). Cells maintained in IL-2 had an increased abundance of proteins required for cytolytic granule fusion with the plasma membrane, such as the GTPase RAB27A, STXBP2 (MUNC18-2), and UNC13D (MUNC13-4) (Fig. 2, F to H). These data indicate that IL-2 may regulate the protein content and release of lytic granules.

IL-2 control of transcriptional regulators and core protein synthesis machinery

Another key function of IL-2 is to regulate and maintain T cell transcriptional programs, in part through the activation of STAT5. Our data indicate that IL-2 may influence gene transcription in both general and specific ways in CTLs by increasing the abundance of multiple transcription factors and proteins involved in transcription and RNA processing, including some components of the general transcriptional machinery, such as TAF1 and TAF8 and TCEB1 (Fig. 3A). Moreover, histone and DNA methylases, DNA and RNA helicases, and some RNA-processing proteins (Fig. 3A), with the exception of proteins involved in methylation of the mRNA cap (Fig. 3A), were all statistically significantly decreased in abundance in CTLs deprived of IL-2. These decreases suggested that the loss of IL-2 signaling would generally reduce gene expression. However, some of the transcription factors reduced in IL-2-deprived cells are gene-specific transcription factors (Fig. 3A and table S2). These included MAFK, NFIL3, and the AP-1 family proteins JUN, JUNB, JUND, and FOSL2, eomesodermin (EOMES), IRF8, and TCF25 (Fig. 3, A and B). However, the abundance of two transcription factors FOXO1 and TBET (Fig. 3C), which are both important for the maintenance of T cell identity (32, 33), were not changed by the loss of IL-2 signals. These data highlight that the ability of IL-2 to control gene transcription and the production and stability of mRNAs in T cells goes beyond stimulation of STAT5 phosphorylation and activity.

The phenotype of a cell is controlled by its transcriptional program but gene expression cannot be executed without protein synthesis. IL-2 has a key role in promoting the rate of protein synthesis in $CD8^+$ T cells (24, 25). Our proteomic analysis revealed that IL-2 influenced protein synthesis on many levels. IL-2 increased the abundance of ribosomal proteins (Fig. 3D) such that CTLs maintained in IL-2 contained ~2.8×10^6 ribosomes, whereas CTLs deprived of IL-2 only had ~1.2×10^6 ribosomes (Fig. 3D). IL-2 also controlled the abundance of tRNA synthases, including the methionyl-tRNA synthase, and sustained the abundance of critical components of the EIF translational initiation complex (Fig. 3E). IL-2 also maintained the abundance of proteins that enable the transport of newly synthesized proteins into the endoplasmic reticulum (ER) and the abundance of proteins

involved in protein folding and protein degradation in both the ER lumen and the cytosol (Fig. 3E). These data suggest that IL-2 coordinates the abundance of ribosomes, translation complexes, and protein quality-control mechanisms.

IL-2 regulation of amino acid transporters and amino acid sensors

A supply of amino acids is required for cells to sustain high rates of protein synthesis. System L transporters are heterodimeric, sodium independent amino acid transporters whose substrates include large neutral amino acids such as leucine, tryptophan and methionine (34). IL-2 sustains system L-mediated amino acid transport in CTLs (35). $CD8^+$ T cells lacking the system L amino acid transporter SLC7A5 fail to differentiate into CTLs (35). Our proteomics data identified SLC7A5 as the most abundant amino acid transporter in CTLs with ~170 000 copies per cell and determined that its abundance depended on IL-2 (Fig. 4A). We quantified ~6 other amino acid transporters in CTLs, including an arginine transporter (SLC7A1) (Fig. 4B) and a transporter for glutamine and serine (SLC1A5) (Fig. 4C). The abundance of all 7 amino acid transporters was maintained by IL-2 (Fig. 4D). IL-2 also increased the abundance of proteins required for amino acid biosynthesis (Fig. 4E) and proteins involved in the recovery of amino acids by autophagy (Fig. 4, F to I). These results indicate that IL-2 maintains the supply of amino acids to CTLs through multiple mechanisms.

In addition to amino acids being vital for the protein biosynthetic capacity of T cells, specific amino acids also are necessary for other essential metabolic processes. For example, serine fuels the biosynthesis of the purine nucleotides needed for T cell proliferation (36); glutamine fuels protein O-GlcNAcylation in T cells (37); arginine promotes oxidative phosphorylation over glycolysis and increases the survival of T cells (38) and, together with leucine, stimulates the activity of mTORC1. Differentiation and maintenance of the cellular mass of $CD8^+$ T cells depend on mTORC1 (20–22). Our data suggest that one mechanism by which IL-2 can sustain high mTORC1 activity in effector CTLs is by maintaining the supply of leucine and arginine. Another mechanism indicated by the data is that IL-2 increases the abundance of proteins that regulate mTORC1 activity (39) (Fig. 4, J to L). Although some of the proteins that IL-2 sustained are parts of negative regulatory complexes, others are positive regulators of mTORC1 (Fig. 4J). For example, IL-2 maintained the abundance of the GTPase RHEB (Fig. 4K) and the cytosolic leucine sensor SESTRIN2 (Fig. 4L).

IL-2 control of glucose metabolism and oxygen sensing

CTLs have high rates of glucose transport, exhibit a high rate of glycolysis, and have a high rate of oxidative phosphorylation. These metabolic programs are required for effector function (23). In our dataset, we found that proteins mapped to oxidative phosphorylation comprised ~1% of the IL-2-maintained CTL proteome by mass (Fig. 5A); proteins of the TCA cycle were ~0.8% of the CTL proteome (Fig. 5B); and glycolytic enzymes were ~9% of the CTL proteome (Fig. 5C). IL-2 deprivation reduced the amount of proteins involved in glucose metabolism, but they retained a similar relative abundance within the cell (Fig. 5, A to C). The rate-limiting step for glucose metabolism in CTLs is glucose transport, and our data showed that IL-2 maintains the abundance of the glucose transporters GLUT1 (also

known as SLC2A1) and GLUT3 (also known as SLC2A3) in CTLs (Fig. 5, D and E). This IL-2-dependent increase in glucose transporters had functional consequences: IL-2-deprived CTLs had reduced glucose uptake compared to that of CTLs maintained in IL-2 (Fig. 5F).

The expression of genes encoding glucose transporters in CTLs is controlled by the HIF1α/HIF1β transcriptional complex (21). IL-2 deprivation caused a decreased abundance of HIF1β (Fig. 5G) and HIF1α, which we measured by Western blotting because HIF1α was not detected by mass spectrometry (Fig. 5H) (21). We previously described HIF1 target genes in CTLs (21). Here, we showed that, in addition to a reduction in the abundance of GLUT1 and GLUT3, other proteins that are encoded by genes stimulated by HIF1, such as perforin (Fig. 2C), TIM-3 (also known as HAVCR2) (Fig. 5I), and NFIL3 (Fig. 5J) were decreased upon IL-2 deprivation. Additionally, we previously established that HIF1 complexes repress expression of the gene encoding the cell adhesion molecule CD62L (L-selectin, SELL) (21). The increase in the abundance of CD62L (Fig. 5K) in IL-2-deprived CTLs was thus consistent with a reduction in the HIF transcriptional program.

In CTLs, the abundance of HIF1α is increased by the activity of the mTORC1 pathway (21). In the presence of high oxygen, the oxygen-dependent proline hydroxylase (PHD) proteins hydroxylate prolines within HIF1α, targeting HIF1α for ubiquitylation by the ubiquitin ligase VHL. This limits the abundance of HIF1α in CTLs when environmental oxygen is high but enables a rapid increase in HIF1α abundance in response to a reduced amount of oxygen in the environment. The oxygen-sensing pathways mediated by PHD proteins and VHL are important for restraining $CD8^+$ T cell immune responses (40). We identified PHD2 as the dominant proline hydroxylase in CTLs and did not detect PHD1 or PHD3. The abundance of PHD2 was maintained by IL-2 (Fig. 5L), highlighting IL-2 as a critical regulator of oxygen-sensing pathways in CTLs.

IL-2 control of the CTL proteome through JAKs

IL-2-induced activation of JAK1 and JAK3 is essential for IL-2 signal transduction. Consequently, we predicted that pharmacological inhibition of JAKs would mimic the effect of IL-2 deprivation and similarly re-shape the CTL proteome. We used mass spectrometry to compare the proteomes of CTLs maintained in IL-2 alone or in the presence of the JAK1/3 inhibitor, Tofacitinib, which is now used clinically to limit JAK1/3 activity in autoimmune diseases (41). We treated CTLs with 100 nM Tofacitinib, which is within the range of Tofacitinib concentrations found in the plasma in patients (42–45). Consistent with previous work (24), 100 nM Tofacitinib decreased the tyrosine phosphorylation of STAT5 in CTLs (Fig. 6A), prevented T cell cycle progression (Fig. 6B), and decreased the size (Fig. 6C) and protein content of CTLs (Fig. 6D), indicating suppression of protein synthesis. CTLs exposed to 100 nM Tofacitinib were viable after 24 hours; higher concentrations of the drug caused losses in cell viability (fig. S2A). By mass spectrometry, we identified ~7000 protein groups in the IL-2-maintained control and Tofacitinib-treated CTLs (fig. S2, B and C and table S3). In each of these datasets, there was good correlation and >87% overlap in the identified proteins between the replicates for each condition (fig. S2, B to E).

Inhibition of JAK1/3 affected the composition of the CTL proteome (Fig. 6E). Tofacitinib decreased the abundance of the IL-2Rα subunit (Fig. 6, F and G) in a response that was very

similar to that observed in cells deprived of IL-2 (fig. S2F and table S4). There were some quantitative differences in the magnitude of protein regulation between Tofacitinib treatment and IL-2 deprivation with IL-2 deprivation tending to produce a stronger reduction in abundance (fig. S2, F to J and table S4). Treatment of IL-2-maintained CTLs with 100 nM Tofacitinib decreased the protein content of CTLs by ~25% (Fig. 6D), whereas IL-2 deprivation caused a ~40% reduction in protein mass (Fig. 1B). However, despite these quantitative differences, inhibition of JAK1/3 with Tofacitinib induced changes to the CTL proteome that were qualitatively comparable to those we observed in response to IL-2 deprivation. For example, JAK1/3 inhibition resulted in a loss of the cell surface proteins IL-4Rα, IL-12Rβ1, and TNFRSF9 (also known as 4-1BB and CD137) (Fig. 6E and fig. S2F). The abundance of key cell cycle regulatory proteins and DNA synthesis machinery was also reduced by JAK1/3 inhibition, with the exception of p27, which increased in abundance in response to both Tofacitinib (Fig. 7A and fig. S2G) and IL-2 deprivation (Fig. 1L). Tofacitinib also replicated the effect of IL-2 deprivation on the protein synthesis machinery and decreased the abundance of ribosomal proteins and proteins required for translation (Fig. 7A and fig. S2, H and I). Inhibition of JAK1/3 mimicked the effect of IL-2 deprivation on the abundance of amino acid transporters (Fig. 7B and fig. S2J) and, similar to IL-2-deprived CTLs, CTLs treated with Tofacitinib decreased the abundance of the mTORC1 pathway leucine sensor, SESTRIN2 (Fig. 7C and fig. S2J). Tofacitinib also decreased the abundances of the HIF1 targets GLUT1 and GLUT3 in CTLs (Fig. 7, D and E and fig. S2J). This correlated with Tofacitinib-treated CTLs having reduced glucose uptake (Fig. 7F) and glycolysis, as determined by measurement of lactate output (Fig. 7G), as compared to IL-2-maintained CTLs. Tofacitinib-treated CTLs also decreased the abundance of other HIF targets, such as perforin (Fig. 7H and fig. S2J) and the transcription factor NFIL3 (Fig. 7I and fig. S2J). The reduction in proteins encoded by HIF-stimulated genes indicated that JAK inhibition also reduced HIF abundance. We confirmed the dependency of HIF1α abundance on JAK activity by Western blotting analysis with selective HIF1α antibodies (Fig. 7J). Together, these data highlight how the ability of IL-2 to shape the T cell proteome depends on JAK catalytic activity; the data also reveal the extent to which a clinically relevant inhibitor of JAK signaling modulates T cell responses to IL-2.

Identification of NFIL3 as a key effector of an IL-2-mediated oxygen-sensing pathway

A challenge with large, unbiased datasets is identifying data that give new biological insights. We applied two strategies to gain new insights. We examined the proteins that had the largest change in protein abundance in IL-2-deprived or Tofacitinib-treated CTLs. We also took a targeted approach based on our previous studies that mapped signaling pathways mediated by mTORC1 and HIF1 complexes in CTLs (21, 23). By applying both filters, the transcription factor NFIL3 emerged as a target for IL-2-JAK1/3-mTORC1-HIF1 signaling. Our proteomics data indicate that NFIL3 was statistically significantly decreased in copy number (Fig. 5J and Fig. 7I) and relative abundance (Fig. 8A) in CTLs in response to IL-2 deprivation or Tofacitinib. We validated these results using the orthogonal approach of Western blotting (Fig. 8B). IL-2 deprivation and Tofacitinib treatment also decreased the relative amount of *Nfil3* mRNA (Fig. 8C), suggesting that transcriptional regulation of NFIL3 contributes to its sustained abundance in IL-2-maintained CTLs.

NFIL3 has critical functions in NK cells (46) and other innate lymphoid cells (ILCs) (47), and CD4$^+$ T cells (48), but *Nfil3* mRNA has not been previously reported as being detected in CD8$^+$ T cells. Therefore, we evaluated the abundance of NFIL3 at the protein and transcript level in naïve and antigen-activated P14 CD8$^+$ T cells. Both NFIL3 protein and *Nfil3* mRNA were either undetectable or at very low abundance in naïve CD8$^+$ T cells (Fig. 8, D and E) and were low, albeit reproducibly detectable, in antigen receptor-activated T cells (Fig. 8, D and E). However, when antigen-activated CD8$^+$ T cells were clonally expanded in IL-2 to produce effector CTLs, *Nfil3* mRNA and protein increased and were sustained at high abundance (Fig. 8, D and E). This is consistent with the model that the induction of NFIL3 is not controlled by TCR activity but depends on IL-2-JAK1/3 signaling.

Our proteomics data indicate a role for oxygen-sensing pathways in the control of *Nfil3* expression. Transcriptional microarray analysis found that *Nfil3* mRNA was decreased in abundance in HIF1β-null CTLs (21). Thus, we evaluated *Nfil3* expression in HIF1α-null (*Hif1a*$^{-/-}$) CTLs. Western blotting analysis indicated that the abundance of NFIL3 in effector CTLs depended on HIF1α and was responsive to changes in oxygen (Fig. 8F). T cells switched from 20% oxygen to 1% oxygen exhibited an increase the abundance of HIF1α and the expression of HIF1 target genes, including those encoding the glucose transporter GLUT1 (SLC2A1) and perforin (21). We found that NFIL3 abundance increased when wild-type, but not *Hif1a*$^{-/-}$, CTLs were switched from 20% oxygen to 1% O_2 (Fig. 8F). This correlated with an increase in *Nfil3* mRNA in CTLs cultured in 1% O_2 compared to that in CTLs cultured in 20% O_2 (Fig. 8G). The effect on *Nfil3* transcripts was comparable to the effect on the abundance of transcripts for GLUT1 in response to a reduction in oxygen (Fig. 8H). Together, these data show that the abundance of NFIL3 in CTLs is regulated by oxygen-sensing pathways controlled by the HIF1 transcription factor complex.

To explore the functional relevance of the regulation of NFIL3 in CTLs, we isolated CD8$^+$ naïve T cells from the spleens of NFIL3-deficient (*Nfil3*$^{-/-}$) mice, activated the TCR, and clonally expanded the cells in IL-2. Activated *Nfil3*$^{-/-}$ CD8$^+$ T cells proliferated normally in response to IL-2 (fig. S3A). Moreover, IL-2-maintained *Nfil3*$^{-/-}$ CD8$^+$ effector T cells upregulated normal amounts of activation markers, such as IL-2Rα, CD69, and CD44 (fig. S3, B to D). They also showed normal activity of AKT and mTORC1, key regulators of CTL differentiation (fig. S3, E and F). We previously reported that HIF1-null effector CD8$^+$ T cells fail to decrease the abundance of CD62L, a key adhesion molecule that controls lymphocyte migration into secondary lymphoid tissue, and are negative for perforin (21). *Nfil3*$^{-/-}$ CD8$^+$ T cells phenocopied HIF1α-null CD8$^+$ T cells and retained high amounts of CD62L (*Sell*) mRNA and protein (Fig. 8, I and J) and failed to express perforin (*Prf1*) mRNA and protein (Fig. 8, K and L). Together, these data identify NFIL3 as a transcription factor whose abundance in CTLs is regulated by HIF1-mediated oxygen-sensing pathways. The data also show that NFIL3 controls perforin abundance in T cells and has a role in the repression of CD62L in antigen- and cytokine-activated CD8$^+$ T cells.

Discussion

Our study provides an in-depth insight into the role of IL-2 in configuring and maintaining the proteome of differentiated CTLs. One key perspective from the proteomic analysis was

the extent to which IL-2-JAK1/3 signaling shapes the ability of effector CTLs to respond to their immune environment. IL-2 controlled the abundance of multiple cell surface molecules, including receptors for the cytokines IL-4 and IL-12, the inhibitory receptor Tim-3 (gene name HAVCR2), and the co-stimulatory receptor, 4-1BB. The signaling pathways controlled by these receptors can substantially modulate T cell responses. Indeed, a 4-1BB agonist antibody, Utomilumab, is in clinical trials to promote effector $CD8^+$ anti-tumor T cell therapy. The recognition that the abundance of 4-1BB is increased by IL-2 is a useful insight into how therapeutic IL-2 treatments may be able to enhance the function of effector T cells.

A further insight from our data was that IL-2 maintained the abundance of proteins that stimulate the differentiation and proinflammatory actions of CTLs in parallel with those that may keep these activities in check, thus potentially maintaining cellular fitness. IL-2 induces a proinflammatory gene expression program by regulating the activity of transcription factors such as STAT5, HIF1α, and NFIL3, by promoting glucose metabolism, and by enhancing protein synthesis. IL-2 stimulates the production of proteins on many levels by regulating the abundance of amino acid transporters, tRNA synthases, ribosomal subunits, core translational machinery, and proteins that coordinate the assembly of translationally competent ribosomal complexes. Maintaining glucose metabolism is likely to be a critical determinant of sustaining the highly energy-consuming processes of ribosomal biogenesis and protein translation in CTLs. Thus, by enhancing metabolism and protein synthesis, IL-2 modulates an indirect regulation of cell phenotype independently of transcriptional networks. In this respect, the data reveal that IL-2 equally sustained the abundance of proteins that destroy mis-folded proteins. Maintaining these protein degradation pathways may be required to prevent the accumulation of damaged proteins and preserve the cellular fitness of these CTLs as they perform the high rates of protein biosynthesis required for rapid cell proliferation and effector function. In a similar way, IL-2 finely tunes the abundance of proteins to prevent aberrant immune responses. For example, IL-2 increased the abundance of 4-1BB, which boosts CTL function, but also increased the abundance of Tim-3 (HAVCR2), which can inhibit CTL function. The ability of IL-2 to control the abundance of stimulatory and inhibitory receptors would, therefore, control the balanced activity of effector T cells.

One fundamental insight from the current data set is the dominant role for IL-2 in controlling how effector T cells respond to their nutrient environment. We found that IL-2 regulated a diverse repertoire of nutrient transporters, including those required for the uptake of glucose, iron, methionine, leucine, serine, arginine, and glutamine. These amino acids are necessary for protein synthesis and for other critical metabolic pathways. IL-2 also maintained the abundance of the amino acid-sensing pathways mediated by the leucine sensor SESTRIN2 that controls mTORC1 activity. The importance of nutrient supply for effector T cell function is now well-recognized, and the effects of IL-2 on maintaining nutrient transporter abundance, therefore, enable IL-2 to have a major role in co-regulating metabolism and protein production in effector $CD8^+$ T cells. In this respect, the fact that more than 3000 proteins did not undergo changes in abundance and that some proteins increased in abundance as a result of IL-2 deprivation seems contradictory to the marked effect of IL-2 on amino acid transport and overall protein synthesis. However, proteomic

data provide a snapshot of cellular protein concentrations that result from the balanced rates of protein synthesis and protein degradation. The proteins that are IL-2-insensitive may well be very stable proteins. Additionally, although IL-2 controls amino acid uptake from the environment, it is well-established that amino acid-deprived cells switch on autophagy to recycle amino acids. Moreover, the overall metabolic stress caused by IL-2 deprivation could result in preferential translation of mRNAs that enable the cell to maintain some core protein constituents.

Another finding from our study was the integration of IL-2 signaling and oxygen-sensing signaling pathways. The importance of oxygen sensing in regulating effector T cell function is increasingly recognized. The HIF1 signaling pathway is a crucial regulator of T cell differentiation and controls the production of glucose transporters, glycolytic enzymes, chemokine receptors, adhesion molecules, and the cytolytic effector molecule, perforin (21, 49). Indeed, an increase in the abundance of HIF1α is linked to enhanced effector $CD8^+$ T cell function (49), whereas reduced PHD protein abundance improves the efficacy of effector T cells in the lung to clear tumor metastases (40). The expression of PHDs in T cells in the lung also suppresses effector T cells to prevent immune-mediated tissue damage (40). Therefore, it is important to understand that IL-2 drives the accumulation of both HIF1α and PHD2.

In this respect, another finding from this study was the convergence of the IL-2 and oxygen sensing signaling pathways. An example of this was the ability of both IL-2 and HIF1 to control the expression of NFIL3, a bZIP family transcriptional repressor, in CTLs. Previous studies showed that NFIL3 is important for the development of NK cells (46) and other ILCs (47). Our finding that NFIL3 is regulated by HIF1 downstream of IL-2 and hypoxia reveals how the expression of this important transcription factor is controlled. Note that we found that the abundance of NFIL3 in CTLs was markedly decreased in response to the JAK1/3 inhibitor Tofacitinib, which is in clinical use. Thus, our data give insights into the molecular details of how these drugs control immune cell function. For example, it would be important to understand whether the JAK kinase-mediated control of oxygen-sensing and HIF1 transcription factors determines NFIL3 expression in NK cells or ILCs. It will also be important to understand the molecular basis for NFIL3 control of $CD8^+$ T cell transcriptional programs in more detail. Indeed, NFIL3 inhibits FOXO-mediated transcriptional programs in HEK 293 cells (50), and FOXOs are critical regulators of $CD8^+$ T cell differentiation and, similar to NFIL3, can control the expression of perforin and CD62L (51, 52). Thus, it will be important to explore whether NFIL3 acts to form a functional link between oxygen-sensing and the control of FOXO transcription factors in T cells.

In summary, our data highlight the multiple ways in which IL-2-JAK signaling can shape the proteomic landscape of effector T cells to control protein metabolism and other key cellular metabolic programs. These data offer a comprehensive understanding of the effect of IL-2 signaling on effector CD8 T cells that explains the powerful immunomodulatory actions of this cytokine. IL-2 controls the fate of regulatory and effector $CD4^+$ T cells; a future challenge will be to understand how IL-2 configures the proteomes of these cells to see if there are distinct effects in different populations.

Materials and Methods

Study plan

This study aimed to define the proteome of in vitro generated CTLs in the presence or absence of IL-2 and the JAK kinase inhibitor Tofacitinib. Three biological replicates were used for proteomic studies Each biological replicate was generated from the spleen of one mouse. Mice were age-matched and sex-matched and were used between 12 and 15 weeks of age. Where possible, cage-mates were used within each experiment. Other experiments were performed as indicated in the figure legends.

Mice

P14 mice have been described previously (26). Female P14 TCR transgenic mice were used for proteomic studies, and both male and female mice were used for other experiments. Mice with floxed *Hif1a* alleles were crossed with mice expressing Cre recombinase under the control of the *Vav* promoter to generate mice with deletion of HIF1α in Vav-expressing cells. *Nfil3*$^{-/-}$ mice have been described previously (46). All mice were bred and maintained in compliance with UK Home Office Animals (Scientific Procedures) Act 1986 guidelines.

In vitro cultures of CTLs

CTLs were generated as described previously (24). Briefly, naïve CD8$^+$ T cells taken from the spleens of mice were activated by triggering of the TCR for 48 hours in the presence of 20 ng/ml IL-2 (Proleukin, Novartis) and 2 ng/ml IL-12 (R and D Systems). P14 mice were activated with 100 ng/ml gp-33 peptide of the Lymphocytic Choriomeningitis Virus (LCMV) and TCR non-transgenic T cells were activated with 0.5μg/ml anti-CD3 (BioLegend) and 0.5μg/ml anti-CD28 (eBioscience). After 48 hours, the activated CD8$^+$ cells were removed from TCR stimulation and were then cultured in RPMI 1640 (Life Technologies), with 10% fetal bovine serum (FBS) (Life Technologies), supplemented with 50 units/ml penicillin-G (GIBCO), 50 μg/ml streptomycin (GIBCO), 50 μM β-mercaptoethanol (Sigma-Aldrich) and 20 ng/ml IL-2 (Proleukin, Novartis). CTLs were differentiated in IL-2 for 4 days before any 24 hour treatments were performed. Samples were considered biological replicates if the CTLs were generated from separate spleens. When required, CD8$^+$ T cells were purified and isolated with the EasySep Mouse CD8$^+$ isolation kit (STEMCELL Technologies) as directed by the manufacturer's instructions.

Inhibitors and cell treatments

Cells were treated with 100 nM Tofacitinib (Selleckchem). Where appropriate, cells were treated with DMSO as controls. To deprive cells of IL-2, cells were pelleted, washed in an excess of pre-warmed medium lacking IL-2 for 5 min before being pelleted and resuspended in pre-warmed medium lacking IL-2. For the IL-2-maintained controls, the CTLs were subjected to the same washes with 20 ng/ml IL-2 being added back before further culturing.

Proteomic sample processing

Following CTL generation and treatment, CTLs were lysed in urea buffer (8 M urea, 50 mM Tris pH 8.0, 1 mM TCEP) with protease (cOmplete mini EDTA free, Roche) and

phosphatase inhibitors (PhosStop, Roche) at room temperature for 30 min. Samples were sonicated, and protein concentration was determined using a BCA assay (Pearce) according to the manufacturer's instructions. To reduce samples, 10 mM DTT was added for 30 min at room temperature. After reduction, 50 mM iodoacetimide was added to each sample and incubated for 45 min at room temperature in the dark. Samples were then diluted to 4 M urea with Tris buffer (100 mM Tris pH 8.0, 1 mM CaCl2). LysC (Wako), reconstituted in Tris buffer, was then added to each sample at a ratio of 50:1 protein:LysC and the samples were incubated with LysC overnight at 30°C. Samples were then transferred to low-bind 15-ml falcon tubes (Eppendorf) and further diluted with Tris buffer to 0.8 M urea. Trypsin (Promega), reconstituted with Tris buffer, was then added to the samples at a ratio of 50:1 protein:trypsin and the samples were incubated for 8 hours at 30°C. After digestion, the samples were desalted with C18 SepPack cartridges (Waters) and dried down in a SpeedVac (Genevac). Dried peptide samples were resuspended in 10 mM sodium borate 20% (v/v) acetonitrile (pH 9.3) and fractionated into 16 fractions by strong anion exchange (SAX) chromatography. Peptide samples for proteomic analysis were fractionated with an Ultimate 3000 HPLC equipped with an AS24 strong anion exchange (SAX) column as previously described (23). For the separation, the buffers used were 10 mM sodium borate (pH 9.3) (SAX buffer A) and 10 mM sodium borate (pH 9.3), 500 mM NaCl (SAX buffer B). Peptide samples were resuspended in 210 µl of 10 mM sodium borate 20% (v/v) acetonitrile (pH 9.3) and injected onto the SAX column and separated using an exponential elution gradient starting with Buffer A. In total, 16 peptide fractions were collected and desalted with Sep-pack C18 96 well desalting plates (Waters). Desalted peptides were dried down with a SpeedVac (Genevac).

Fractions were desalted and dried, resuspended in 1% formic acid, and separated by nanoscale C18 reverse phase chromatography (Ultimate 3000 RSLC nano system, Thermo Scientific) before being electrosprayed into the Linear Trap Quadrupole-Orbitrap mass spectrometer (LTQ-Orbitrap Velos Pro; Thermo Scientific). The chromatography buffers used were as follows: HPLC Buffer A (0.1% formic acid), HPLC Buffer B (80% acetonitrile, 0.08% formic acid), and HPLC Buffer C (0.1% formic acid). Peptides were loaded onto an Acclaim PepMap100 nanoViper C18 trap column (100 µm inner-diameter, 2 cm; Thermo Scientific) in HPLC Buffer C with a constant flow of 5 µl/min. After trap enrichment, peptides were eluted onto an EASY-Spray PepMap RSLC nanoViper, C18, 2 µm, 100 Å column (75 µm, 50 cm; Thermo Scientific) using the following buffer gradient: 2% B (0 to 3 min), 2 to 40% B (3 to 128 min), 40 to 98% B (128 to 130 min), 98% B (130 to 150 min), 98-2% B (150 to 151 min), and equilibrated in 2% B (151 to 180 min) at a flow rate of 0.3 µl/min. The eluting peptide solution was automatically electrosprayed into the coupled Linear Trap Quadrupole-Orbitrap mass spectrometer (LTQ-Orbitrap Velos Pro; Thermo Scientific) using an Easy-Spray nanoelectrospray ion source at 50°C and a source voltage of 1.9 kV (Thermo Scientific). The mass spectrometer was operated in positive ion mode. Full-scan MS survey spectra (m/z 335 to 1800) in profile mode were acquired in the Orbitrap with a resolution of 60,000. Data were collected using data-dependent acquisition: the fifteen most intense peptide ions from the preview scan in the Orbitrap were fragmented by collision-induced dissociation (normalized collision energy, 35%; activation Q, 0.250; and activation time, 10 ms) in the LTQ after the accumulation of 5000 ions. Precursor ion

charge state screening was enabled and all unassigned charge states as well as singly charged species were rejected. The lock mass option was enabled for survey scans to improve mass accuracy. Mass spectrometry was performed by the Proteomics facility, University of Dundee, UK.

Proteomic data processing and analysis

The mass spectrometry data files were processed with MaxQuant version 1.6.0.1 and the spectra were mapped to the reviewed UniProtKB mouse protein database and the contaminant database supplied by MaxQuant. The following search parameters were used: trypsin and LysC were selected as the proteases; up to two missed cleavages were permitted; the minimum peptide length was set to six amino acids; protein N-terminal acetylation, methionine oxidation, glutamine to pyroglutamate, and glutamine and asparagine deamidation were selected as variable modifications; carbamindolyation of cysteine residues was set as a fixed modification; MS tolerance of 20 ppm and MS/MS tolerance of 0.5 Daltons; label-free quantification was enabled. False discovery rates (FDRs) were set to 0.01 and based on hits against the reversed sequence database. This cut-off was applied to individual spectra and whole proteins in the MaxQuant output. The match between runs function was enabled. Proteins were quantified on the basis of unique (found only in a specific protein group) and razor peptides (peptides assigned to a specific protein group without being unique to that group) with the requantification feature enabled.

After processing of the files by MaxQuant, Perseus software implementing the proteome ruler plug-in was used to calculate estimated copy numbers of proteins per cell. This analysis assigns the copy numbers of histones in a diploid mouse cell to the summed peptide intensities of all histones in a sample to estimate copy numbers for all identified proteins in the dataset (28). The accuracies of the quantification were annotated based according to the number of peptides and the percentage of unique peptides identified for the protein as follows: high: ≥ 8 peptides detected, minimum of 75% unique peptides; medium: ≥ 3 peptides detected, a minimum of 50% unique peptides; low: all other peptides. Data quality was assessed by evaluating peptide intensities for normal distribution, the overlap in protein identification, and the correlation of the estimated copy number between replicates. The output from MaxQuant was filtered to remove known contaminants, those proteins identified as part of a reversed protein library, and proteins identified only by a modified site. To evaluate changes to the proteome resulting from the loss of IL-2-JAK1/3 signaling, the estimated copy numbers were used to determine the ratio of the abundance of individual proteins within biological replicates. The statistical significance of these changes was determined by performing a one-sample t-test, without further adjustment, on the ratios of the treated condition:IL-2-maintained condition. Proteins were defined as being statistically significantly regulated in abundance if they had a ratio of ≥ 1.5 or ≤ 0.67 and a P value of ≤ 0.05.

Western blotting

Cells were lysed in RIPA buffer (50 mM Tris pH 7.4, 1% NP-40, 0.5% sodium deoxycholate, 0.1% SDS, 150 mM NaCl, 2 mM EDTA, 50 mM NaF, 20 mM TCEP) with cOmplete mini EDTA-free protease inhibitor tablets (Roche) for 10 min at 4°C. The

resulting lysates were sonicated and then mixed with NuPAGE LDS sample buffer supplemented with TCEP before being heated to 70°C for 10 min. Samples were separated on an SDS-PAGE gel using the Mini-PROTEAN Tetra Cell system. The proteins were then transferred to nitrocellulose membranes (Hybond-C Extra, Amersham). Membranes were incubated with the following primary antibodies: STAT5A/B (CST #9363), STAT5A/B pTyr^{694}/pTyr^{699} (CST, #9359), NFIL3 (CST #14312), granzyme B (CST #4275), perforin-1 (CST #3693), HIF-1α (R&D Systems, clone 241809, cat. MAB15361), SMC1 (Bethyl labs, cat. A300-005A), S6 pSer^{235}/pSer^{236} (CST #2211), S6 (CST #2217), S6K pThr^{389} (CST #9205), S6K (CST #9202), AKT pThr^{308} (CST #4056), AKT pSer^{473} (CST #4058), AKT (CST #9272), FOXO1/3A pThr^{24}/pThr^{32} (CST #9464), and FOXO1 (CST #9454).

Primary antibodies were detected with HRP-conjugated secondary antibodies (goat anti-rabbit, Thermo Scientific #31460; goat anti-mouse, Thermo Scientific #31430), and chemiluminescence was detected using X-ray films (Konica) or an Odyssey Fc Imaging System (LI-COR). ImageJ software (NIH) was used to quantify chemiluminescence captured on film and Image Studio Software (LI-COR) was used to quantify chemiluminescence detected using the Odyssey system. Total protein bands of interest were normalized to SMC1 loading controls, then for each blot, each band was normalized to a control sample. Phosphorylated protein bands of interest were normalized to the total protein band and normalized to a control sample.

Cell staining and flow cytometry

Cells were stained with saturating concentrations of the following antibodies: IL-2Rα (CD25, BD BioScience, clone PC61; or BD Pharmingen, clone 7D4), CD69 (eBioscience, clone HI.2F3), CD44 (BD Pharmingen, clone IM7), CD62L (BD Pharmingen, MEL-14), CD4 (eBioscience, clone RM4-5), CD8 (BioLegend, clone 53-6.7). Data were acquired on a FACS Verse flow cytometer with FACSuite software (BD Biosciences) or a FACS LSR Fortessa flow cytometer with DIVA software (BD Biosciences). Viable cells were gated according to their forward- and side-scatter profiles. Data analysis was performed with FlowJo software (Treestar). To compare surface protein abundance from multiple experiments, the geometric mean fluorescence intensity (GeoMFI) was determined. If all data were recorded in the same experiment, raw GeoMFI data were shown. If data were recorded in separate experiments, the data for each experiment were normalized to controls for presentation.

RNA extraction and qPCR

RNA was isolated with the Qiagen RNeasy kit and cDNA was generated using the Quantabio cDNA synthesis kit. RT-PCR was performed with the SYBRgreen dye (BioRad) on an iCycler iQ PCR machine. *Tbp*, *Cd8a* and *Hprt1* were used as the reference genes as indicated in the figure legends. Data were analyzed using the ΔΔCT method. Primers were *Cd8a* forward: 5'-GATATAAATCTCCTGTCTGCCCATC-3'; *Cd8a* reverse: 5'-ATTCATACCACTTGCTTCCTTGC-3'; *Sell* forward: 5'-CCTGTAGCCGTCATGGTCAC-3'; *Sell* reverse: 5'-GAATCAGTATGGATCATCCATC-3'; *Slc2a1* forward: 5'-CCAGCAGCAAGAAGGTGA-3'; *Slc2a1* reverse: 5'-ATGTTTGATTGTAGAACTCCTC-3'; *Hprt1* forward: 5'-

TGATCAGTCAACGGGGGACA-3'; *Hprt1* reverse: 5'-TTCGAGAGGTCCTTTTCACCA-3'; *Nfil3* forward: 5'-GCGATGGTAGCCGGAAGTTGC-3'; *Nfil3* reverse: 5'-CCTGTGCGGGGCTTTCCTGAG-3'; Prf1 forward: 5'-CGTCTTGGTGGGACTTCAG-3'; *Prf1* reverse: 5'-GCATTCTGACCGAGTGGCAG-3'; *Tbp* forward: 5'-GGGGAGCTGTGATGTGAAGT-3'; *Tbp* reverse: 5'-CCAGGAAATAATTCTGGCTCAT-3'.

Glucose uptake

The measurement of radiolabelled glucose uptake has been described previously (21). Briefly, glucose-free RMPI 1640 medium labelled with 0.5 μCi/ml radiolabelled 2-deoxy-d-[1-3H]glucose (Perkin Elmer) was layered over 500 μl of a 1:1 mixture of silicone oil (Sigma Aldrich) and dibutyl phthalate (Sigma Aldrich). Cells (1 x 106 per measurement) were added and allowed to take up radiolabelled 2-deoxy-d-[1-3H]glucose for 4 min. The cells were then lysed in 100 mM NaOH and the radioactivity was analyzed using a Beckman LS 6500 Multi-Purpose Scintillation Counter (Beckman Coulter). Assays were performed in duplicate or triplicate per biological replicate. For each biological replicate, data were normalized to the uptake of 2-deoxy-d-[1-3H]glucose in the IL-2-maintained CTL sample.

Lactate output

Lactate measurements were performed as described previously (21). CTLs were resuspended to a concentration of 2 x 10^6 cells/ml in RPMI with 10% (v/v) dialyzed serum and incubated for 4 hours, after which the supernatants were collected. Lactate concentration was determined using an enzymatic assay in which the oxidation of lactate by lactate dehydrogenase (LDH) is monitored by the change in absorption at 340 nm after the reduction of NAD+ to NADH. To determine the lactate concentration, equal volumes of supernatant and master mix (320 mM glycine, 320 mM hydrazine, 2U lactate dehydrogenase and 2.4mM NAD^+) were mixed and incubated for 10 min at room temperature. Absorbance of the reactions was then read at 340 nm with a cytofluor II Fluorescence Multi-Well Plate Reader (Perceptive BioSystems). A lactate standard curve was generated and the concentration of lactate in the test samples was inferred after data analysis with Prism software (GraphPad).

Statistical analyses

Statistical analyses on protein changes from the proteomic data were performed as outlined in the proteomics methods section. Further data derived from the proteomic studies (such as the estimated number of ribosomes per cell) and validation data were subjected to similar statistical analyses: the ratios of the treated condition:IL-2-maintained condition were determined and subjected to a two-tailed, one-sample t-test, without further adjustment. For studies comparing T cells with gene knockouts to wild-type T cells, two-tailed unpaired, unequal variance t-tests were used.

Supplementary Material

Refer to Web version on PubMed Central for supplementary material.

Acknowledgments

We thank Cantrell group members and Jens Hukelmann for their critical discussion of the data, the Biological Resources unit, Flow Cytometry facility (M. Lee, A. Whigham, R. Clarke), Proteomics Facility (D. Lamont and team), and Data Analysis Group (Dr M. Gierlinski, for statistics support) at the University of Dundee.

Funding: Work was supported by the Wellcome Trust (Principal Research Fellowship 097418/Z/11/Z and 205023/Z/16/Z to D.A.C.) and Tenovus Scotland (S.H.R). C.M.R. was the recipient of a studentship from the Biotechnology and Biological Sciences Research Council (BBSRC) and GlaxoSmithKline.

References and Notes

1. Liao W, Lin J-X, Leonard WJ. Interleukin-2 at the crossroads of effector responses, tolerance, and immunotherapy. Immunity. 2013; 38:13–25. [PubMed: 23352221]
2. Liao W, Lin J-X, Leonard WJ. IL-2 family cytokines: new insights into the complex roles of IL-2 as a broad regulator of T helper cell differentiation. Curr Opin Immunol. 2011; 23:598–604. [PubMed: 21889323]
3. Cheng G, Yu A, Malek TR. T-cell tolerance and the multi-functional role of IL-2R signaling in T-regulatory cells. Immunological Reviews. 2011; 241:63–76. [PubMed: 21488890]
4. Arenas-Ramirez N, Woytschak J, Boyman O. Interleukin-2: Biology, Design and Application. Trends Immunol. 2015; 36:763–777. [PubMed: 26572555]
5. Boyman O, Sprent J. The role of interleukin-2 during homeostasis and activation of the immune system. Nat Rev Immunol. 2012; 12:180–190. [PubMed: 22343569]
6. Rosenberg SA. IL-2: the first effective immunotherapy for human cancer. J Immunol. 2014; 192:5451–5458. [PubMed: 24907378]
7. Rosenberg SA, Restifo NP. Adoptive cell transfer as personalized immunotherapy for human cancer. Science. 2015; 348:62–68. [PubMed: 25838374]
8. Mitra S, Ring AM, Amarnath S, Spangler JB, Li P, Ju W, Fischer S, Oh J, Spolski R, Weiskopf K, Kohrt H, et al. Interleukin-2 activity can be fine tuned with engineered receptor signaling clamps. Immunity. 2015; 42:826–838. [PubMed: 25992859]
9. Spangler JB, Tomala J, Luca VC, Jude KM, Dong S, Ring AM, Votavova P, Pepper M, Kovar M, Garcia KC. Antibodies to Interleukin-2 Elicit Selective T Cell Subset Potentiation through Distinct Conformational Mechanisms. Immunity. 2015; 42:815–825. [PubMed: 25992858]
10. Gillis S, Smith KA. Long term culture of tumour-specific cytotoxic T cells. Nature. 1977; 268:154–156. [PubMed: 145543]
11. Gillis S, Baker PE, Ruscetti FW, Smith KA. Long-term culture of human antigen-specific cytotoxic T-cell lines. J Exp Med. 1978; 148:1093–1098. [PubMed: 308989]
12. Manjunath N, Shankar P, Wan J, Weninger W, Crowley MA, Hieshima K, Springer TA, Fan X, Shen H, Lieberman J, von Andrian UH. Effector differentiation is not prerequisite for generation of memory cytotoxic T lymphocytes. J Clin Invest. 2001; 108:871–878. [PubMed: 11560956]
13. Kalia V, Sarkar S, Subramaniam S, Haining WN, Smith KA, Ahmed R. Prolonged interleukin-2Ralpha expression on virus-specific CD8+ T cells favors terminal-effector differentiation in vivo. Immunity. 2010; 32:91–103. [PubMed: 20096608]
14. Pipkin ME, Sacks JA, Cruz-Guilloty F, Lichtenheld MG, Bevan MJ, Rao A. Interleukin-2 and Inflammation Induce Distinct Transcriptional Programs that Promote the Differentiation of Effector Cytolytic T Cells. Immunity. 2010; 32:79–90. [PubMed: 20096607]
15. Obar JJ, Molloy MJ, Jellison ER, Stoklasek TA, Zhang W, Usherwood EJ, Lefrancois L. CD4+ T cell regulation of CD25 expression controls development of short-lived effector CD8+ T cells in primary and secondary responses. Proc Natl Acad Sci USA. 2010; 107:193–198. [PubMed: 19966302]
16. Malek TR, Castro I. Interleukin-2 receptor signaling: at the interface between tolerance and immunity. Immunity. 2010; 33:153–165. [PubMed: 20732639]
17. O'Shea JJ, Schwartz DM, Villarino AV, Gadina M, McInnes IB, Laurence A. The JAK-STAT pathway: impact on human disease and therapeutic intervention. Annu Rev Med. 2015; 66:311–328. [PubMed: 25587654]

18. Owen DL, Farrar MA. STAT5 and CD4 (+) T Cell Immunity. F1000Res. 2017; 6:32. [PubMed: 28163905]
19. Preston GC, Sinclair LV, Kaskar A, Hukelmann JL, Navarro MN, Ferrero I, MacDonald HR, Cowling VH, Cantrell DA. Single cell tuning of Myc expression by antigen receptor signal strength and interleukin-2 in T lymphocytes. EMBO J. 2015; 34:2008–2024. [PubMed: 26136212]
20. Sinclair LV, Finlay D, Feijoo C, Cornish GH, Gray A, Ager A, Okkenhaug K, Hagenbeek TJ, Spits H, Cantrell DA. Phosphatidylinositol-3-OH kinase and nutrient-sensing mTOR pathways control T lymphocyte trafficking. Nat Immunol. 2008; 9:513–521. [PubMed: 18391955]
21. Finlay DK, Rosenzweig E, Sinclair LV, Feijoo-Carnero C, Hukelmann JL, Rolf J, Panteleyev AA, Okkenhaug K, Cantrell DA. PDK1 regulation of mTOR and hypoxia-inducible factor 1 integrate metabolism and migration of CD8+ T cells. Journal of Experimental Medicine. 2012; 209:2441–2453. [PubMed: 23183047]
22. Powell JD, Pollizzi KN, Heikamp EB, Horton MR. Regulation of Immune Responses by mTOR. Annu Rev Immunol. 2012; 30:39–68. [PubMed: 22136167]
23. Hukelmann JL, Anderson KE, Sinclair LV, Grzes KM, Murillo AB, Hawkins PT, Stephens LR, Lamond AI, Cantrell DA. The cytotoxic T cell proteome and its shaping by the kinase mTOR. Nat Immunol. 2016; 17:104–112. [PubMed: 26551880]
24. Ross SH, Rollings C, Anderson KE, Hawkins PT, Stephens LR, Cantrell DA. Phosphoproteomic Analyses of Interleukin 2 Signaling Reveal Integrated JAK Kinase-Dependent and -Independent Networks in CD8(+) T Cells. Immunity. 2016; 45:685–700. [PubMed: 27566939]
25. Cornish GH, Sinclair LV, Cantrell DA. Differential regulation of T-cell growth by IL-2 and IL-15. Blood. 2006; 108:600–608. [PubMed: 16569767]
26. Pircher H, Bürki K, Lang R, Hengartner H, Zinkernagel RM. Tolerance induction in double specific T-cell receptor transgenic mice varies with antigen. Nature. 1989; 342:559–561. [PubMed: 2573841]
27. Tyanova S, Temu T, Cox J. The MaxQuant computational platform for mass spectrometry-based shotgun proteomics. Nat Protoc. 2016; 11:2301–2319. [PubMed: 27809316]
28. Wiśniewski JR, Hein MY, Cox J, Mann M. A "proteomic ruler" for protein copy number and concentration estimation without spike-in standards. Mol Cell Proteomics. 2014; 13:3497–3506. [PubMed: 25225357]
29. Smith KA, Cantrell DA. Interleukin 2 regulates its own receptors. Proc Natl Acad Sci USA. 1985; 82:864–868. [PubMed: 2983318]
30. Dimova DK, Dyson NJ. The E2F transcriptional network: old acquaintances with new faces. Oncogene. 2005; 24:2810–2826. [PubMed: 15838517]
31. Jenkins MR, Griffiths GM. The synapse and cytolytic machinery of cytotoxic T cells. Curr Opin Immunol. 2010; 22:308–313. [PubMed: 20226643]
32. Joshi NS, Cui W, Chandele A, Lee HK, Urso DR, Hagman J, Gapin L, Kaech SM. Inflammation directs memory precursor and short-lived effector CD8(+) T cell fates via the graded expression of T-bet transcription factor. Immunity. 2007; 27:281–295. [PubMed: 17723218]
33. Hess Michelini R, Doedens A, Goldrath AW, Hedrick SM. Differentiation of CD8 memory T cells depends on Foxo1. Journal of Experimental Medicine. 2013; 210:1189–1200. [PubMed: 23712431]
34. Mastroberardino L, Spindler B, Pfeiffer R, Skelly PJ, Loffing J, Shoemaker CB, Verrey F. Amino-acid transport by heterodimers of 4F2hc/CD98 and members of a permease family. Nature. 1998; 395:288–291. [PubMed: 9751058]
35. Sinclair LV, Rolf J, Emslie E, Shi Y-B, Taylor PM, Cantrell DA. Control of amino-acid transport by antigen receptors coordinates the metabolic reprogramming essential for T cell differentiation. Nat Immunol. 2013; 14:500–508. [PubMed: 23525088]
36. Ma EH, Bantug G, Griss T, Condotta S, Johnson RM, Samborska B, Mainolfi N, Suri V, Guak H, Balmer ML, Verway MJ, et al. Serine Is an Essential Metabolite for Effector T Cell Expansion. Cell Metab. 2017; 25:345–357. [PubMed: 28111214]
37. Swamy M, Pathak S, Grzes KM, Damerow S, Sinclair LV, Van Aalten DMF, Cantrell A. Glucose and glutamine fuel protein O-GlcNAcylation to control T cell self-renewal and malignancy. Nat Immunol. 2016; 17:712–720. [PubMed: 27111141]

38. Geiger R, Rieckmann JC, Wolf T, Basso C, Feng Y, Fuhrer T, Kogadeeva M, Picotti P, Meissner F, Mann M, Zamboni N, et al. L-Arginine Modulates T Cell Metabolism and Enhances Survival and Anti-tumor Activity. Cell. 2016; 167:829–842.e13. [PubMed: 27745970]
39. Saxton RA, Sabatini DM. mTOR Signaling in Growth, Metabolism, and Disease. Cell. 2017; 168:960–976. [PubMed: 28283069]
40. Clever D, Roychoudhuri R, Constantinides MG, Askenase MH, Sukumar M, Klebanoff CA, Eil RL, Hickman HD, Yu Z, Pan JH, Palmer DC, et al. Oxygen Sensing by T Cells Establishes an Immunologically Tolerant Metastatic Niche. Cell. 2016; 166:1117–1131.e14. [PubMed: 27565342]
41. Smolen JS, Landewé R, Bijlsma J, Burmester G, Chatzidionysiou K, Dougados M, Nam J, Ramiro S, Voshaar M, van Vollenhoven R, Aletaha D, et al. EULAR recommendations for the management of rheumatoid arthritis with synthetic and biological disease-modifying antirheumatic drugs: 2016 update. Annals of the Rheumatic Diseases. 2017; 76:960–977. [PubMed: 28264816]
42. Dowty ME, Jesson MI, Ghosh S, Lee J, Meyer DM, Krishnaswami S, Kishore N. Preclinical to clinical translation of tofacitinib, a Janus kinase inhibitor, in rheumatoid arthritis. J Pharmacol Exp Ther. 2014; 348:165–173. [PubMed: 24218541]
43. Lundquist LM. Efficacy and safety of tofacitinib for treatment of rheumatoid arthritis. WJO. 2014; 5:504. [PubMed: 25232526]
44. Krishnaswami S, Boy M, Chow V, Chan G. Safety, tolerability, and pharmacokinetics of single oral doses of tofacitinib, a Janus kinase inhibitor, in healthy volunteers. Clin Pharmacol Drug Dev. 2015; 4:83–88. [PubMed: 27128212]
45. Lamba M, Wang R, Fletcher T, Alvey C, Kushner J, Stock TC. Extended-Release Once-Daily Formulation of Tofacitinib: Evaluation of Pharmacokinetics Compared With Immediate-Release Tofacitinib and Impact of Food. J Clin Pharmacol. 2016; 56:1362–1371. [PubMed: 26970526]
46. Gascoyne DM, Long E, Veiga-Fernandes H, de Boer J, Williams O, Seddon B, Coles M, Kioussis D, Brady HJM. The basic leucine zipper transcription factor E4BP4 is essential for natural killer cell development. Nat Immunol. 2009; 10:1118–1124. [PubMed: 19749763]
47. Xu W, Domingues RG, Fonseca-Pereira D, Ferreira M, Ribeiro H, Lopez-Lastra S, Motomura Y, Moreira-Santos L, Bihl F, Braud V, Kee B, et al. NFIL3 orchestrates the emergence of common helper innate lymphoid cell precursors. Cell Rep. 2015; 10:2043–2054. [PubMed: 25801035]
48. Motomura Y, Kitamura H, Hijikata A, Matsunaga Y, Matsumoto K, Inoue H, Atarashi K, Hori S, Watarai H, Zhu J, Taniguchi M, et al. The transcription factor E4BP4 regulates the production of IL-10 and IL-13 in CD4+ T cells. Nat Immunol. 2011; 12:450–459. [PubMed: 21460847]
49. Doedens AL, Phan AT, Stradner MH, Fujimoto JK, Nguyen JV, Yang E, Johnson RS, Goldrath AW. Hypoxia-inducible factors enhance the effector responses of CD8(+) T cells to persistent antigen. Nat Immunol. 2013; 14:1173–1182. [PubMed: 24076634]
50. Keniry M, Pires MM, Mense S, Lefebvre C, Gan B, Justiano K, Lau YKI, Hopkins B, Hodakoski C, Koujak S, Toole J, et al. Survival factor NFIL3 restricts FOXO-induced gene expression in cancer. Genes Dev. 2013; 27:916–927. [PubMed: 23630076]
51. Finlay DK, Sinclair LV, Feijoo C, Waugh CM, Hagenbeek TJ, Spits H, Cantrell DA. Phosphoinositide-dependent kinase 1 controls migration and malignant transformation but not cell growth and proliferation in PTEN-null lymphocytes. J Exp Med. 2009; 206:2441–2454. [PubMed: 19808258]
52. Macintyre AN, Finlay D, Preston G, Sinclair LV, Waugh CM, Tamas P, Feijoo C, Okkenhaug K, Cantrell DA. Protein kinase B controls transcriptional programs that direct cytotoxic T cell fate but is dispensable for T cell metabolism. Immunity. 2011; 34:224–236. [PubMed: 21295499]

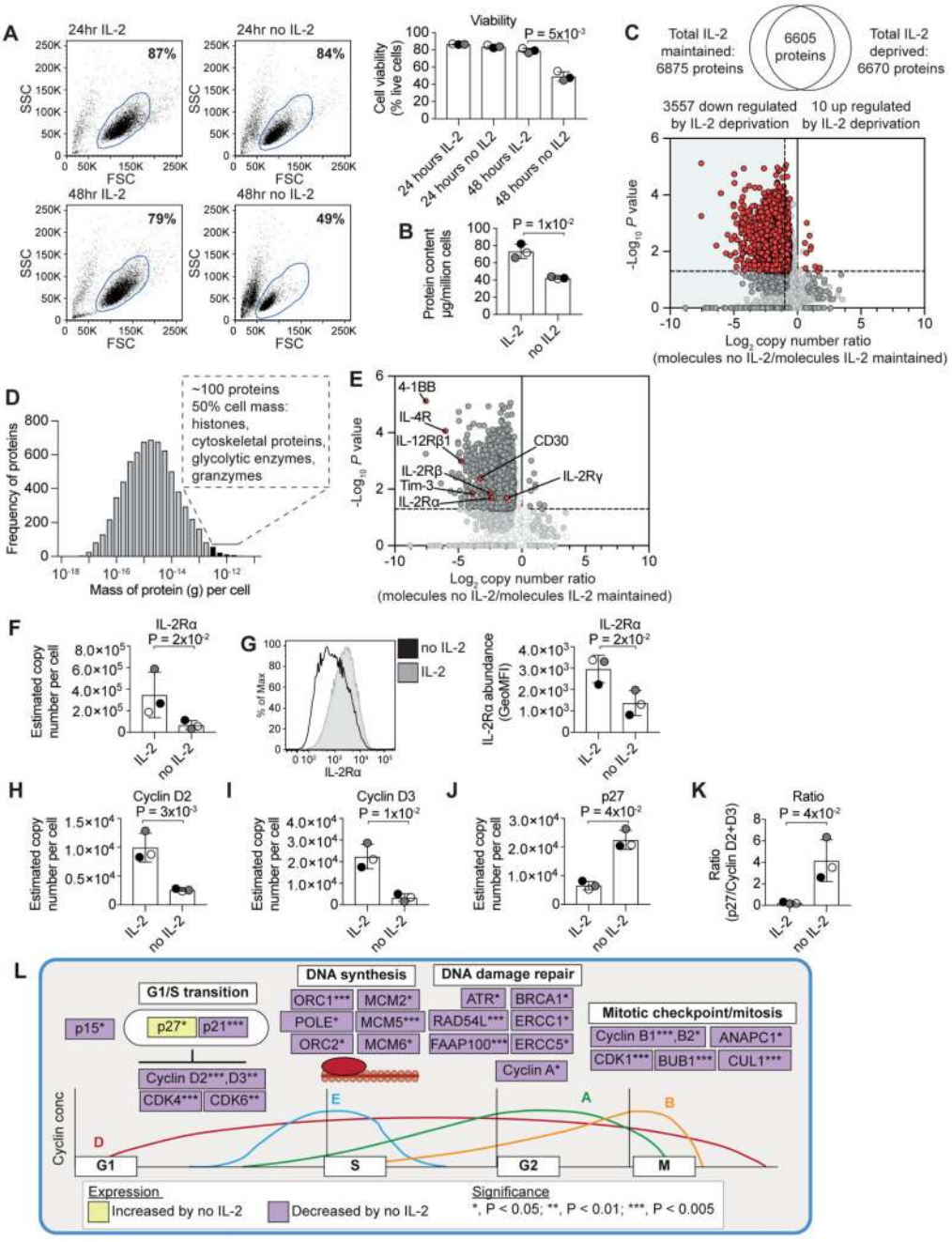

Fig. 1. IL-2 regulation of the CTL proteome.

(**A**) Size and viability of CTL maintained or deprived of IL-2 as judged by flow cytometry forward scatter (FSC) and side scatter (SSC). The percentage of viable CTL are shown alongside. (**B**) Protein content of IL-2 maintained and IL-2 deprived CTL. (**C**) The Venn diagram shows the commonality of proteins identified in the proteomic analysis, and the volcano plot shows the ratio of the protein copy number in CTL deprived of IL-2 for 24 hours compared to IL-2-maintained CTL. Proteins significantly changed (one sample Student's t-test $P < 0.05$) by greater that 1.5-fold are shown in red. A 2-fold decrease in

protein abundance is indicated by the vertical dashed line. (**D**) Average protein mass frequency per cell - bins containing the proteins that make up ~50% of the total CTL mass are shown in black. (**E**) Volcano plot as in (**C**), with surface receptors shown in red. (**F**) Molecule numbers, estimated from the proteomic data, for the abundance of IL-2Rα. (**G**) Flow cytometric analysis of IL-2Rα cell surface abundance. The graph alongside shows the geometric mean fluorescence intensity (GeoMFI) for three biological replicates. (**H** to **J**) Copy numbers estimated from the proteomic data. (**K**) The ratio of p27 to the total sum of Cyclin D2 and Cyclin D3 molecules was calculated and plotted. (**L**) Schematic representation of selected cell cycle proteins, and DNA synthesis and repair enzymes regulated by IL-2. Data show, or are representative of, three biological replicates. In bar charts, data points from biological replicates are color matched, the bar shows the mean and the errors bars show standard deviation. P values shown are two-tailed one sample Student's t-test performed on the ratios of no IL-2 (IL-2 deprived)/IL-2 (IL-2 maintained).

Europe PMC Funders Author Manuscripts

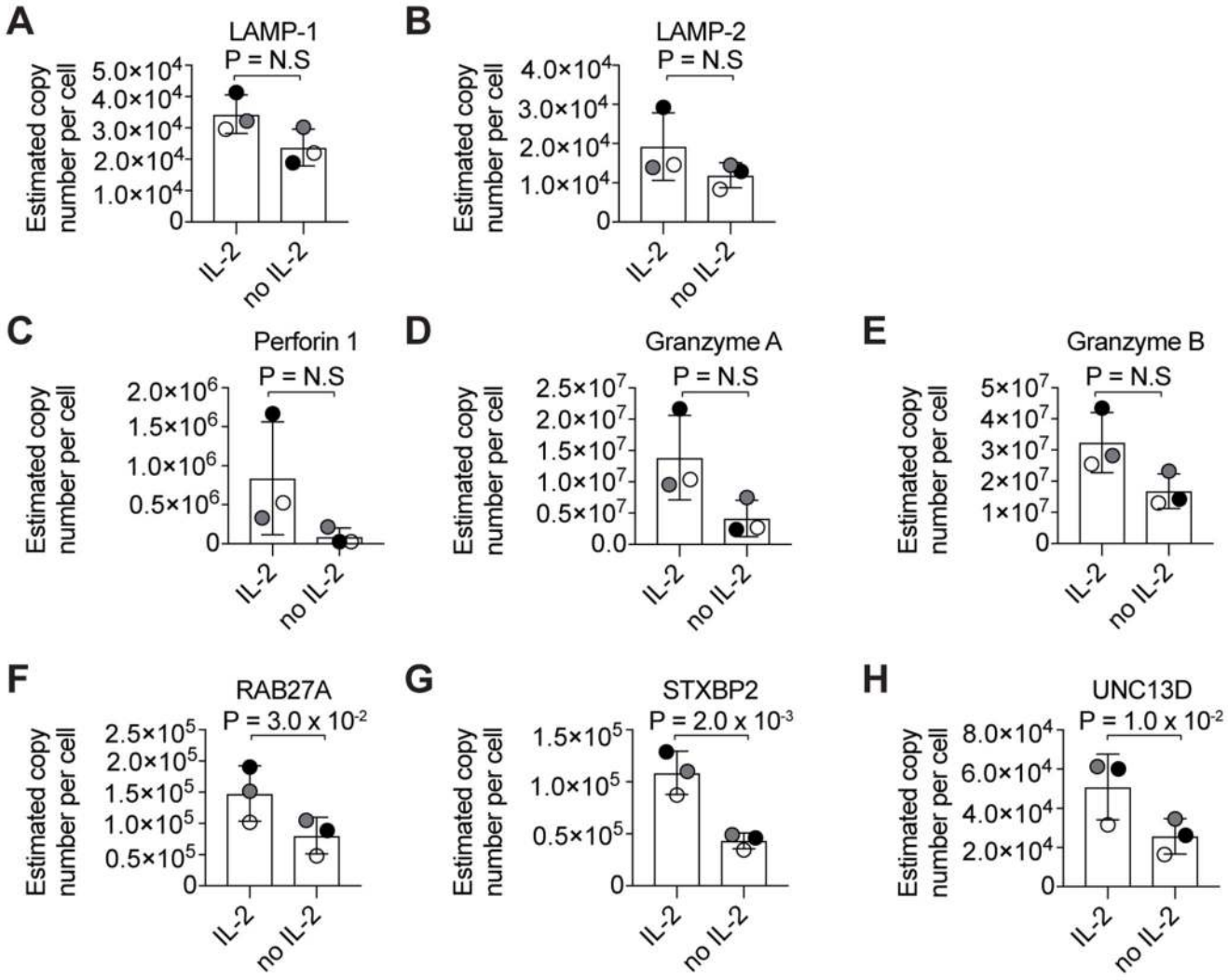

Fig. 2. IL-2 regulation of CTL cytolytic machinery.

(**A** to **H**) Copy numbers estimated from the proteomic data for LAMP-1 (A), LAMP-2 (B), Perforin 1 (C), Granzyme A (D), Granzyme B (E), RAB27A (F), STXBP2 (G), and UNC13D (H). In graphs, the three biological replicates are color-matched, the bar shows the mean and errors bars show standard deviation. P values shown are two-tailed one sample Student's t-test performed on the ratios of no IL-2/IL-2.

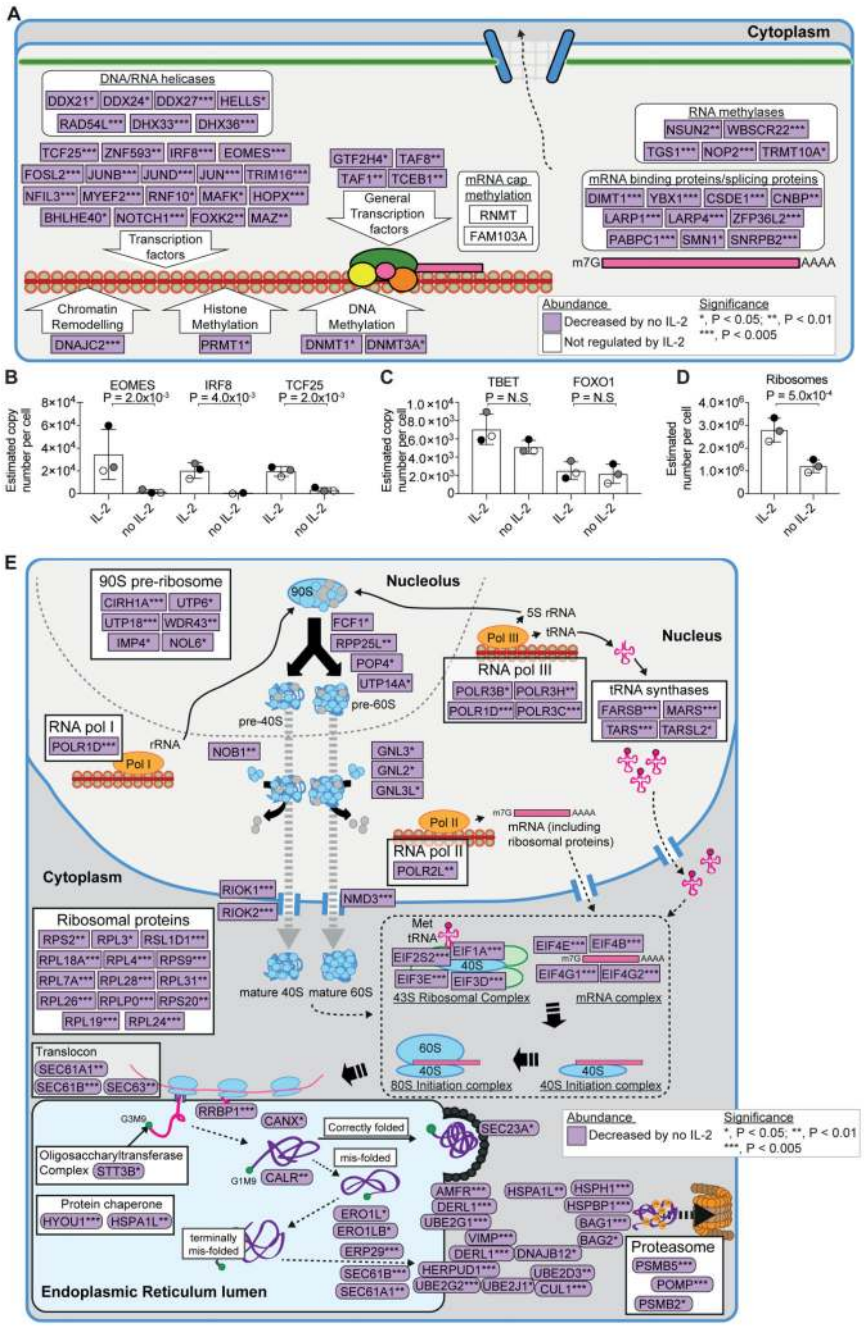

Fig. 3. IL-2 regulation of gene expression.

(**A**) Schematic representation of selected transcription factors, DNA-modifying enzymes and mRNA-binding proteins identified by mass spectrometry in CTLs. (**B** and **C**) Copy numbers estimated from the proteomic data for eomesodermin (EOMES), IRF8, TC25, TBET (TBX21), and FOXO1. (**D**) The number of ribosomes per cell was estimated by calculating the median copy number of all the proteins annotated with the KEGG pathway “ribosome” for each biological replicate and each condition and were plotted in a bar chart. (**E**) Schematic representation of selected proteins involved in ribosomal biogenesis, translation,

and protein processing in the endoplasmic reticulum. In graphs, individual data points from the three biological replicates performed for the proteomic analysis are shown and color matched, with the bar showing the mean and the errors bars showing standard deviation of the experiments. P values shown are two-tailed one sample Student's t-test performed on the ratios of no IL-2/IL-2.

Europe PMC Funders Author Manuscripts

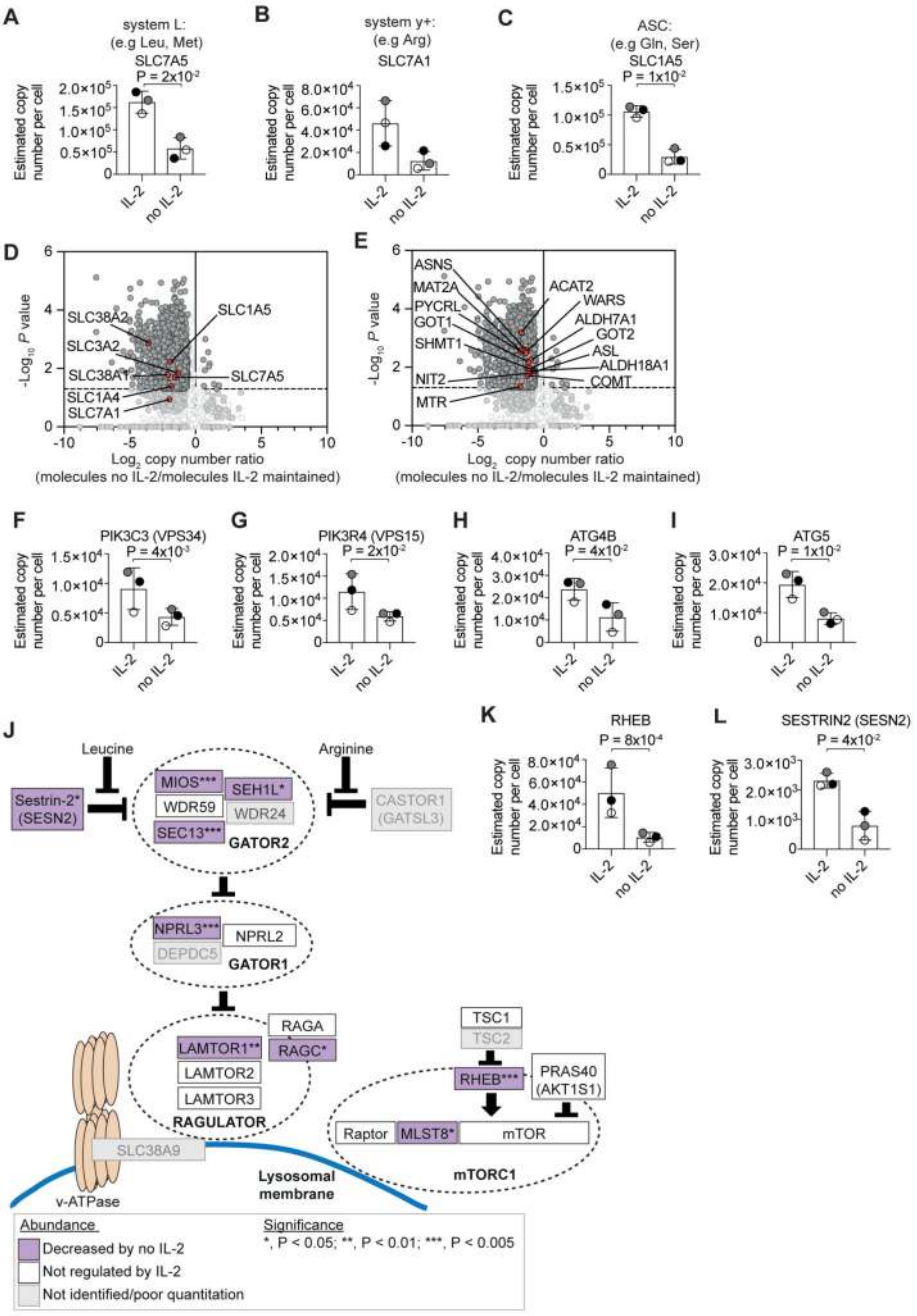

Fig. 4. IL-2 regulation of amino acid uptake and biosynthesis and mTORC1.

(**A** to **C**) Copy numbers estimated from the proteomic data for the amino acid transporter SLC7A5 (A), SLC7A1 (B), and SLC1A5 (C). (D) and (E) Volcano plots of the IL-2-dependent proteome: ratio of the protein abundance (copy number) in IL-2-deprived CTLs compared to IL-2-maintained CTLs is plotted against P value (one sample Student's t-test). Proteins with ratios that are significantly regulated ($P < 0.05$) by greater than 1.5-fold are shown in dark grey, with amino acid transporters highlighted in red in (D) and proteins involved in amino acid biosynthesis in (E). (**F** to **I**) Bar graphs show estimated copy

numbers calculated using the proteomic data for VPS34 (F), VPS15 (G), ATG4B (H) and ATG5 (I). (**J**) Schematic representation of proteins involved in activation of mTORC1 signaling. Proteins decreased in abundance by loss of IL-2 are highlighted in purple. (**K** and **L**) Estimated copy numbers per cell for RHEB (K) and SESTRIN2 (L). In graphs (A)-(C), (F)-(I) and (K)-(L), individual data points from the three biological replicates performed for the proteomic analysis are shown and color matched, with the bar showing the mean and the errors bars showing standard deviation of the experiments. P values shown are two-tailed one sample Student's t-test performed on the ratios of no IL-2/IL-2.

Europe PMC Funders Author Manuscripts

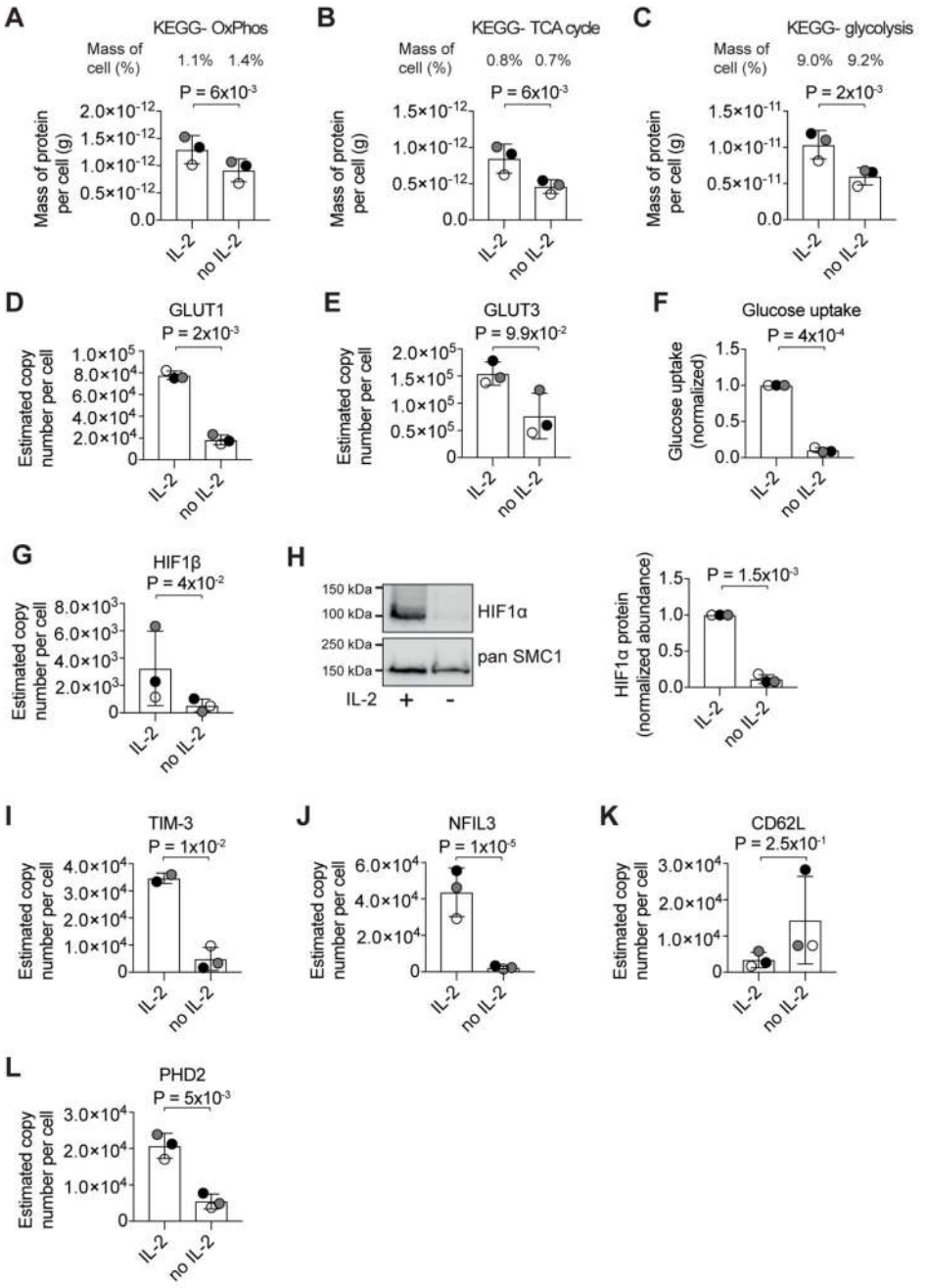

Fig. 5. IL-2 regulation of cellular energy generation.

(**A** to **C**) Graphs show the estimated mass of proteins annotated with the KEGG pathway terms "oxidative phosphorylation" (OxPhos) (A), "TCA cycle" (B), or "glycolysis" (C) per cell in IL-2-maintained and IL-2-deprived CTLs. Estimated mass per protein was determined using estimated copy numbers calculated from the proteomic data using the histone ruler method. The bar charts in (**D**)-(**E**), (**G**) and (**I**)-(**L**) show estimated copy numbers per cell for GLUT1 (SLC2A1) (**D**), GLUT3 (SLC2A3) (**E**), HIF1β (**G**), TIM-3 (**I**), NFIL3 (**J**), L-selectin (CD62L) (**K**) and PHD2 (**L**). (**F**) Glucose uptake in IL-2-maintained

and IL-2-deprived CTLs was measured using radiolabeled 2-deoxyglucose. Data were normalized to glucose uptake in IL-2 maintained CTL. (**H**) HIF1α abundance in CTL in the presence and absence of IL-2 was measured by immunoblot. Quantification of HIF1α detected by Western blot is shown alongside, with data normalized to SMC1 intensity and HIF1α protein abundance in IL-2 maintained CTL. In bar charts, individual data points from the three biological replicates are shown and color matched, with the bar showing the mean and the errors bars showing standard deviation of the experiments. P values shown are two-tailed one sample Student's t-test performed on the ratios of no IL-2/IL-2.

Europe PMC Funders Author Manuscripts

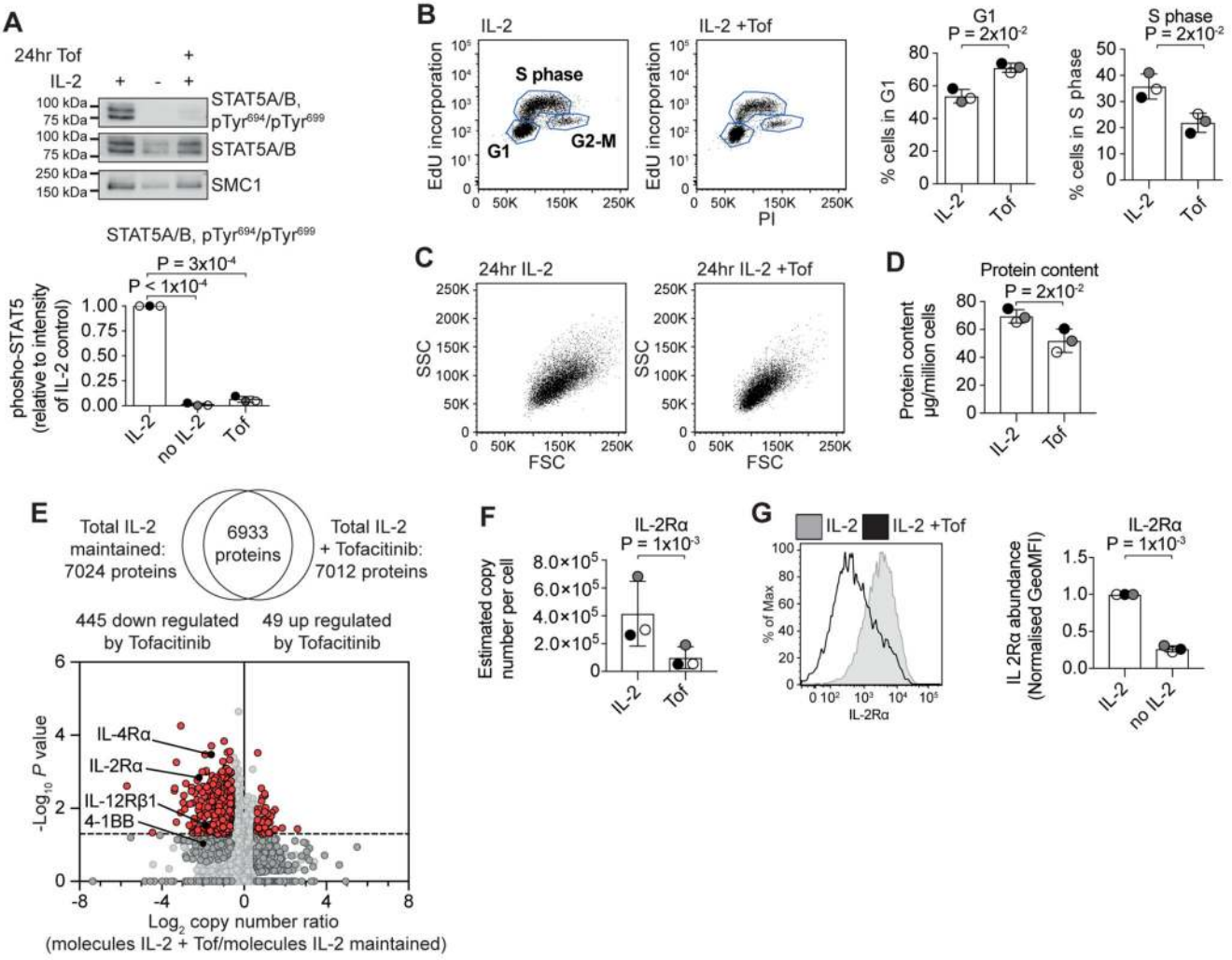

Fig. 6. The impact of Tofacitinib on CTL.

(**A**) Western blot of STAT5A and STAT5B phosphorylation in response to 100 nM Tofacitinib treatment. Quantification of phosphorylated STAT5A and STAT5B is shown below. (**B**) Flow cytometric analysis of cell cycle stages using EdU incorporation into DNA. The percentage of CTLs identified as in G1 and S are shown alongside. Flow cytometry profiles (**C**) and protein content (**D**) of IL-2-maintained CTLs treated with or without Tofacitinib for 24 hours. (**E**) The Venn diagram shows the commonality of proteins identified in the proteomic analysis, and the volcano plot shows the ratio of the protein copy number in IL-2-maintained CTLs treated with 100 nM Tofacitinib for 24 hours compared to IL-2-maintained CTLs is plotted against P value (one sample Student's t-test). Proteins with ratios that are significantly regulated ($P < 0.05$) by greater that 1.5-fold are shown in red with selected surface proteins labeled. IL-2Rα abundance as measured by the proteomic data (**F**) and flow cytometry (**G**) with or without Tofacitinib for 24 hours. The graph alongside shows the normalized geometric mean fluorescence intensity (GeoMFI) for three biological replicates. The data show, or are representative of, three biological replicates. In bar charts, data points from biological replicates are color matched, the bar shows the mean

Europe PMC Funders Author Manuscripts

and the errors bars show standard deviation. P values shown are two-tailed one sample Student's t-test performed on the ratios of IL-2+Tofacitinib/IL-2.

Europe PMC Funders Author Manuscripts

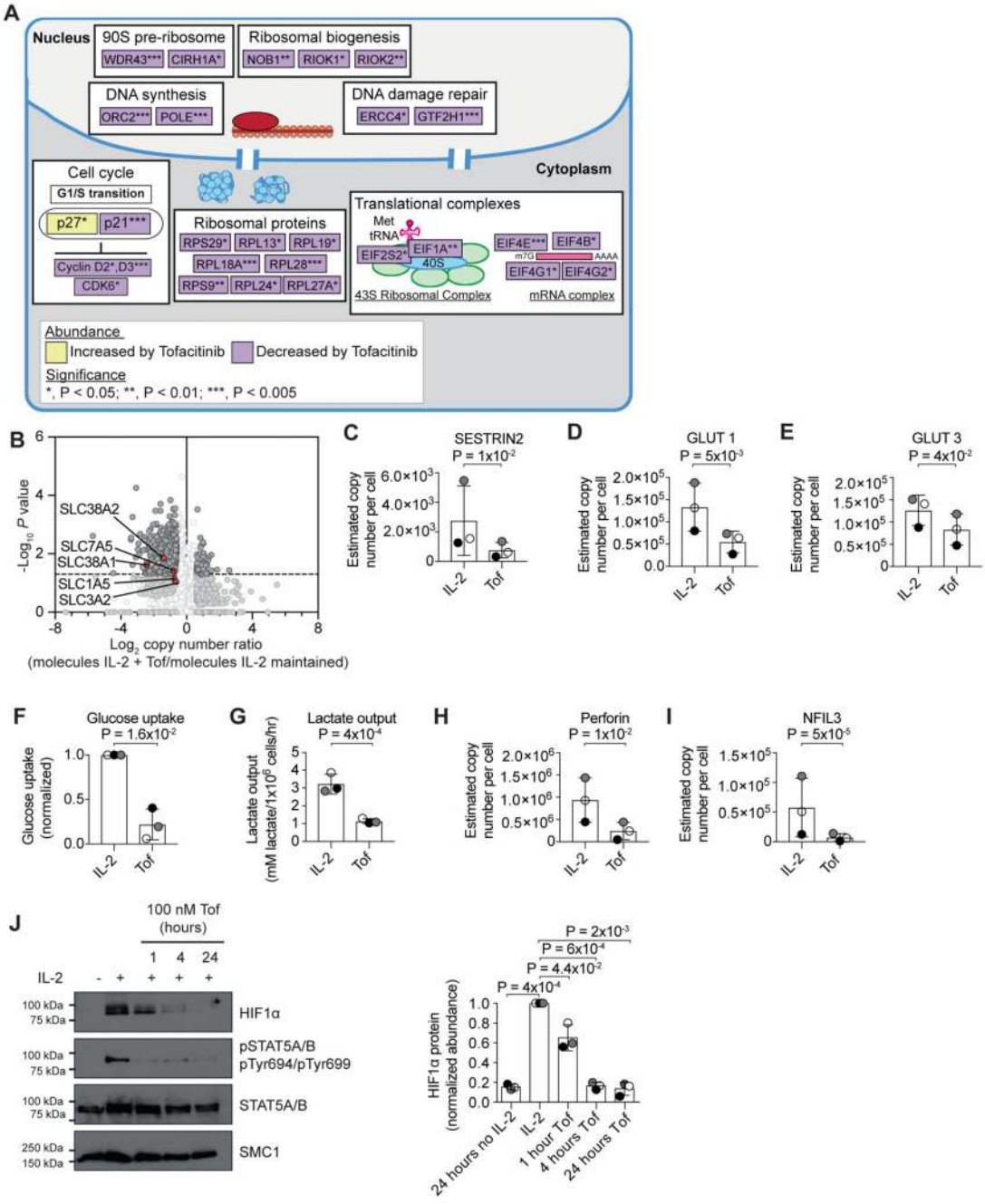

Fig. 7. The Tofacitinib-regulated CTL proteome.

(**A**) Schematic representation of selected molecules regulated by Tofacitinib. (**B**) Volcano plot showing the protein copy number ratio in IL-2-maintained CTLs treated with 100 nM Tofacitinib for 24 hours compared to IL-2-maintained CTLs, significantly regulated proteins are shown in dark grey and nutrient transporters are highlighted in red. Estimated copy numbers per cell are shown for SESTRIN2 (**C**), GLUT1 (**D**) and GLUT3 (**E**). (**F**) Uptake of a radiolabelled glucose analog shown relative to IL-2. (**G**) Lactate output in IL-2-maintained and Tofacitinib-treated CTLs. Estimated copy numbers per cell for perforin (**H**) and NFIL3

Europe PMC Funders Author Manuscripts

(**I**). (**J**) Western blot analysis of HIF1α abundance in response to 100 nM Tofacitinib. Quantification of HIF1α detected by Western blot is shown alongside, with data normalized to SMC1 intensity and HIF1α protein abundance in IL-2 maintained CTL. The data show, or are representative of, three biological replicates. In bar charts, data points from biological replicates are color matched, the bar shows the mean and the errors bars show standard deviation. P values shown are two-tailed one sample Student's t-test performed on the ratios of IL-2+Tofacitinib/IL-2.

Europe PMC Funders Author Manuscripts

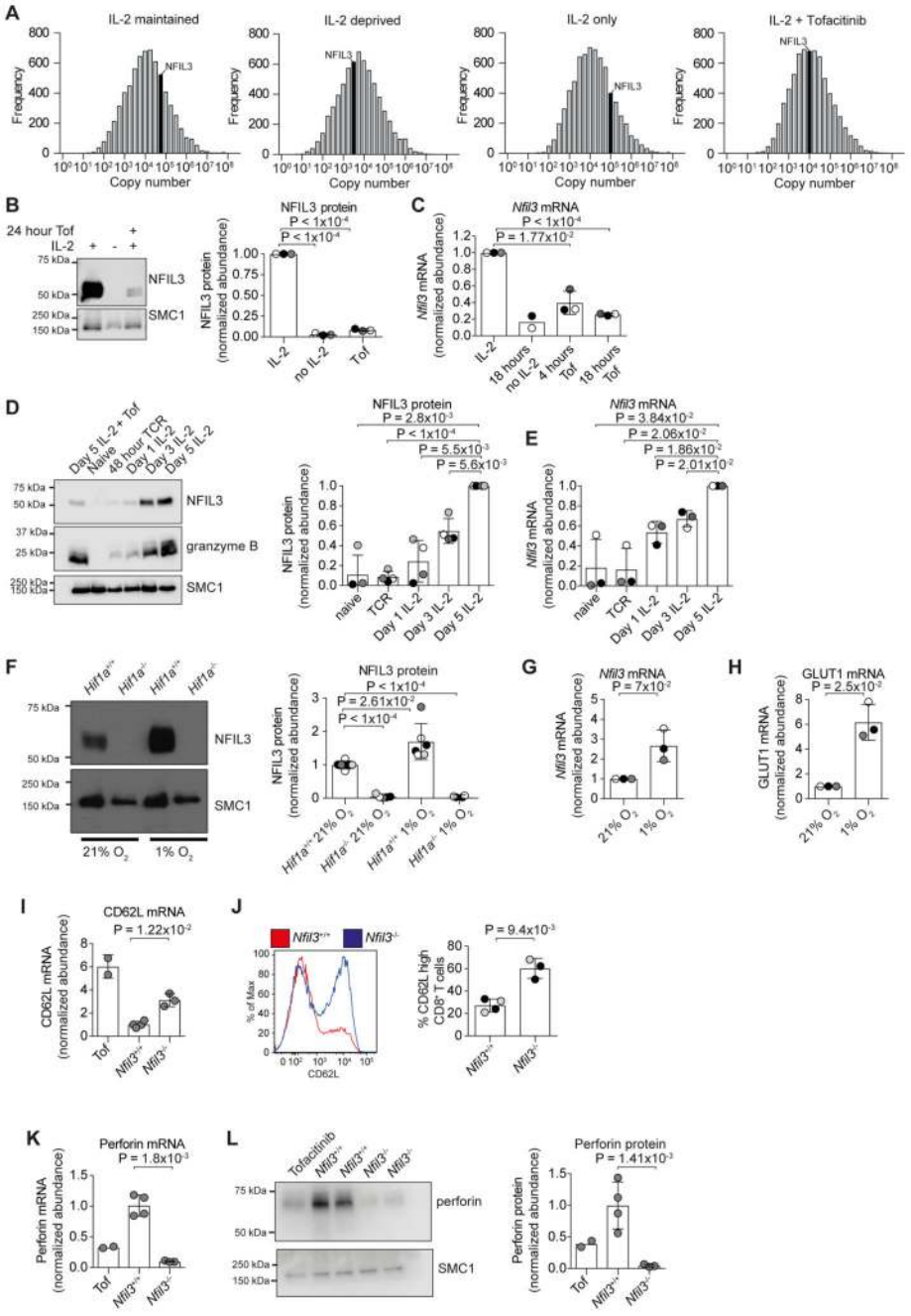

Fig. 8. Regulation of NFIL3 by IL-2-JAK1/3 signaling.

(**A**) Average frequency of protein copy numbers per cell calculated from the proteomic datasets: The bin that contains NFIL3 is indicated in black. (**B**) Western blot analysis of NFIL3 abundance in CTLs following IL-2 deprivation or treatment with 100 nM Tofacitinib. Quantification is shown alongside as data normalized to SMC1 intensity and NFIL3 protein abundance in IL-2 maintained CTL. (**C**) Abundance of *Nfil3* mRNA in CTLs. Abundance of NFIL3 protein (**D**) and mRNA (**E**) in naïve $CD8^+$ T cells, TCR-activated $CD8^+$ T cells, and CTLs activated for 48 hours and then maintained in IL-2 for 1 day, 3 days, or 5 days. (**F**)

Europe PMC Funders Author Manuscripts

Europe PMC Funders Author Manuscripts

Analysis of NFIL3 protein abundance in HIF1α expressing (*Hif1a*$^{+/+}$) and HIF1α deficient (*Hif1a*$^{-/-}$) CTLs maintained in normoxia (21% O_2) or switched into hypoxic (1% O_2) conditions for eight hours. Quantification of NFIL3 protein is shown alongside. Relative abundance of *Nfil3* (**G**) and GLUT1 (*Slc2a1*) (**H**) mRNA in CTLs maintained in normoxia or switched into 1% O_2 for four hours. Abundance of CD62L (*Sell*) mRNA (**I**) and cell-surface protein abundance (**J**) in IL-2-maintained *Nfil3*$^{+/+}$ and *Nfil3*$^{-/-}$ CTL. In (**J**), the percentage of CD8^{+} CD62L high CTLs are shown alongside. Abundance of perforin (*Prf1*) mRNA (**K**) and protein (**L**) in *Nfil3*$^{+/+}$ and *Nfil3*$^{-/-}$ CTLs. In (**L**) quantification of NFIL3, normalized to SMC1 and perforin protein abundance in IL-2 maintained CTL, detected by Western blot is shown alongside. In (**C**), (**G**), and (**H**) the qPCR data were normalized to *Tbp*, and mRNA abundance in IL-2 maintained CTL in normoxia. In (**E**) qPCR data were normalized to *Tbp* and *Cd8* and all are shown relative to day 5 IL-2-maintained CTLs in normoxia. In (**I**) and (**K**), mRNA was normalized to *Hprt*, and data are shown relative to the abundance in *Nfil3*$^{+/+}$ CTLs. Data in (**A**)-(**E**) and (**G**)-(**H**) data show, or are representative of, three biological replicates; in (**F**) data are representative of six *Hif1a*$^{+/+}$ and five *Hif1a*$^{-/-}$ biological replicates, four independent experiments; in (**I**)-(**L**) data are representative of four *Nfil3*$^{+/+}$ and three *Nfil3*$^{-/-}$ biological replicates. Bar charts show data from individual biological replicates, color matched where appropriate, the bar shows the mean and the errors bars show standard deviation. P values shown in (**B**)-(**H**) are two-tailed one sample Student's t-tests and in (**I**)-(**L**) are two-tailed unpaired unequal variance Student's t-tests.